International Journal of Pharmaceutics

Nanostructured TPS/PVA/CNC Films for Sustained Copper Oxide Nanoparticle Release: Toward Advanced Transdermal Dressing Systems

--Manuscript Draft--

Manuscript Number:	IJPHARM-D-25-00100
Article Type:	Research Paper
Section/Category:	Pharmaceutical Nanotechnology
Keywords:	Thermoplastic starch; Sustained release; Transdermal dressings; Cellulose nanocrystals; Copper oxide nanoparticles
Corresponding Author:	Amanda de Sousa Martinez de Freitas, Ph.D. Federal University of Sao Paulo BRAZIL
First Author:	Amanda de Sousa Martinez de Freitas, Ph.D.
Order of Authors:	Amanda de Sousa Martinez de Freitas, Ph.D.
	Jéssica de Souza Rodrigues
	Sofia Municoy
	Pablo E. Antezana
	Martín F. Desimone
	María Laura Foresti
	Marystela Ferreira
	Ana Paula Lemes
Abstract:	There is a constant search to create alternatives to replace traditional dressings with biodegradable materials. Furthermore, it is desired that these materials present good performance properties, low cost, easy processing, and a controlled release of actives. In this sense, nanocomposites films of thermoplastic starch (T) with different percentages (10, 20, 30 and 40% m/V of polyvinyl alcohol (P) and reinforced with 2.5; 5.0 and 10% (m/m) of cellulose nanocrystals (CNC) were optimized by casting technique for transdermal dressings application. The nanocomposites film with the best properties were additivated with copper oxide nanoparticles (NPCuO), aiming to study the controlled release of these nanoparticles by the dressing. The synthesis and characterization of NPCuO was also carried out. The final material developed (T/P/10CNC/NPCuO) was extensively characterized, with measurements of thickness, swelling capacity in PBS buffer, tensile test, contact angle measurements, thermogravimetric analysis (TGA) and Fourier-transform infrared spectroscopy (FTIR). In addition, solubility, water vapor permeation, NPCuO release by visible ultraviolet spectroscopy (UV-Vis) and the cytocompatibility of the developed films were studied. The results showed that the nanocomposites films had adequate thickness for application in dressings, with good swelling capacity in PBS buffer and flexibility. In addition, the material showed good solubility in PBS, permeability within the standards of commercial dressings, sustained release capacity of nanoparticles used for 8 hours, and desirable cytocompatibility, with cell proliferation for 48 hours. Due to the characteristics of the optimized film, it was considered a promising material for application as transdermal dressings with controlled release of actives.
Suggested Reviewers:	Pascal Wong-Wah-Chung pascal.wong-wah-chung@univ-amu.fr
	Xuetao Guo guoxuetao2005@nwafu.edu.cn
	Jean-Luc Gardette luc.gardette@univ-bpclermont.fr
	Luc Averous Averous

	luc.averous@unistra.fr

Nanostructured TPS/PVA/CNC Films for Sustained Copper Oxide Nanoparticle Release: Toward Advanced Transdermal Dressing Systems

Amanda de S. M. de Freitas[a,b*], Jéssica de S. Rodrigues[b], Sofia Municoy[c], Pablo E. Antezana[c], Martín F. Desimone[c], María Laura Foresti[d], Marystela Ferreira[b], Ana Paula Lemes[a]

[a] Polymers and Biopolymers Technology Laboratory (TecPBio), Institute of Science and Technology (ICT), Federal University of São Paulo (UNIFESP), São José do Campos, Brazil

[b] Science and Technology Center for Sustainability (CCTS), Federal University of São Carlos (UFSCar), Sorocaba, Brazil

[c] Institute of Chemistry and Drug Metabolism (IQUIMEFA), University of Buenos Aires (UBA), National Council for Scientific and Technical Research (CONICET), Faculty of Pharmacy and Biochemistry, Buenos Aires, Argentina

[d] Instituto de Tecnología em Polímeros y Nanotecnología, University of Buenos Aires (UBA), National Council for Scientific and Technical Research (CONICET), Laboratorio de Materiales y Estructuras (LAME), Buenos Aires, Argentina

[*]Corresponding author: amandasmf91@gmail.com

ABSTRACT

There is a constant search to create alternatives to replace traditional dressings with biodegradable materials. Furthermore, it is desired that these materials present good performance properties, low cost, easy processing, and a controlled release of actives. In this sense, nanocomposites films of thermoplastic starch (T) with different percentages (10, 20, 30 and 40% m/V of polyvinyl alcohol (P) and reinforced with 2.5; 5.0 and 10% (m/m) of cellulose nanocrystals (CNC) were optimized by casting technique for transdermal dressings application. The nanocomposites film with the best properties were additivated with copper oxide nanoparticles (NPCuO), aiming to study the controlled release of these nanoparticles by the dressing. The synthesis and characterization of NPCuO was also carried out. The final material developed (T/P/10CNC/NPCuO) was extensively characterized, with measurements of thickness, swelling capacity in PBS buffer, tensile test, contact angle measurements, thermogravimetric analysis (TGA) and Fourier-transform infrared spectroscopy (FTIR). In addition, solubility, water vapor permeation, NPCuO release by visible ultraviolet spectroscopy (UV-Vis) and the cytocompatibility of the developed films were studied. The results showed that the nanocomposites films had adequate thickness for application in dressings, with good swelling capacity in PBS buffer and flexibility. In addition, the material showed good solubility in PBS, permeability within the standards of commercial dressings, sustained release capacity of nanoparticles used for 8 hours, and desirable cytocompatibility, with cell proliferation for 48 hours. Due to the characteristics of the optimized film, it was considered a promising material for application as transdermal dressings with controlled release of actives.

Keywords: Thermoplastic starch, Sustained release, Transdermal dressings, Cellulose nanocrystals, Copper oxide nanoparticles.

1. Introduction

The search for the development of alternative materials with less impact on the environment is urgent. For this, biodegradable materials have been widely studied, since they can be decomposed in nature in a shorter period of time when compared to traditionally applied materials [1]. In this context, one of the polymers with great potential in the development of these products is starch. However, materials produced from native starch have characteristics that hinder their application in various segments of the industry, such as low thermal stability, inferior mechanical properties and low tolerance to moisture and aging [2]. Therefore, modifications in native starch are desirable, not only to solve these deficiencies, but also to develop other properties of interest.

Among the possible modifications are the addition of plasticizers [3], mixing with other biopolymers, [4] and/or nano reinforcements, [5] that result in the formation of thermoplastic starch, blends and polymeric nanocomposites, respectively. Usually two plasticizers are combined and used with the native starch to promote the plastification of starch and produce TPS. A volatile plasticizer (water) and a non-volatile plasticizer (such as: glycerol, sorbitol, urea, citric acid, among others), generating a material with better processability [6,7].

The polyvinyl alcohol (PVA) is widely used polymer for the production of TPS blends because it is a water-soluble polymer, excellent film former, viscosity modifier and adhesive [8]. In addition, PVA is a non-toxic, non-carcinogenic, and biocompatible material, characteristics that favor the controlled release of drugs [9]. It is transparent, biodegradable, and offers protection against ultraviolet rays, [10] being chemically and thermally stable [11]. PVA contributes positively to properties related to water interactions, such as solubility and materials. Several studies are reported in the literature describing the development of blends and composites of starch and PVA, for various applications, including the form of foams, [10] smart films, [8] nanofibers [11] and even as surface modifiers [12].

The incorporation of nanofillers to this TPS/PVA blend is a strategy, highlighting the use of CNC. Reinforcing TPS/PVA films with cellulose nanocrystals (CNC) is a promising strategy to enhance their physicochemical properties for biomedical applications. The incorporation of CNC increases the rigidity and mechanical strength of the material, resulting in more durable films that are ideal for transdermal dressings and controlled drug delivery systems. Additionally, the CNC improve thermal stability and moisture barrier properties, contributing to the integrity and functionality of the films in humid environments, such as wounds [13]. The formation of this nanocomposite becomes attractive to the biomedical industry due to the biocompatibility and biodegradability of the materials obtained and the

versatility of presentation in the form of hydrogels, [14] films [15] and scaffolds [16]. Cellulose nanocrystals are highly crystalline particles, with a diameter of 5 to 30 nm and the appearance of needles, but their characteristics may vary according to the type of vegetable and the extraction method [15,17,18]. These nanofillers have low density, high rigidity and mechanical strength when compared to other fillers commonly used in polymeric matrices such as glass fibers, for example [19,20]. Thus, the CNC are able to improve the properties of the material or even confer new properties, acting as a structural mechanical reinforcement, in the capacity and cell proliferation, [13] and in the biodegradability, [21] of starch-based materials.

The formed nanocomposites blend can be an alternative to the use of synthetic polymers for biomedical applications, more specifically in the field of dressings, with the advantage of being biocompatible and biodegradable, since the dressing material is used for a relatively short period and then has to be discarded [22]. The treatment of wounds with a dressing consists of using this physical resource or chemical-drugs as a transdermal possibility for accelerating healing, encouraging the production of fibroblasts, promoting a proteolytic remodeling of the extracellular matrix [9]. It is also important that the dressings are easy to remove so that they do not generate secondary injuries or pain in the removal process.

The healing material can be also improved through the insertion of metallic nanoparticles, conferring bactericidal, antimicrobial and antioxidant properties [14]. Among the main nanoparticles used are those of metallic iron oxides, [23] copper, [24,25] titanium, [26] zirconium, and silver [27–29]. Copper oxide nanoparticles were chosen in this study due to their antimicrobial and antioxidant properties, which are highly interesting as a tool to be explored against the antibiotic resistance crisis, attributed to the excessive and improper use of these drugs [24]. In addition, another advantage is its non-toxicity, low cost and longer delivery time [23].

Thus, the plastification of starch with glycerol and water allowed obtaining TPS which, together with PVA and CNC, were used for the development of the nanocomposite. To the optimized product, with better performance properties, NPCuO were added. Therefore, it was important to establish adequate conditions to produce the nanocomposite, seeking the optimization and standardization of the methodology to obtain reproducible results that allowed the development of the curative material.

This study differs from others reported in the literature because it is focused on the development of a transdermal dressing from the conception of the idea. Therefore, all the analyses carried out were extremely focused on the application. Even so, there was a concern with the choice of biopolymers, the optimization of the proportions used. In addition to the

study of the ideal amount of nanofillers used and the incorporation of copper oxide nanoparticles. The work sought to cover the physical-chemical characterization of the developed material, as well as to carry out specific tests for the application. Being the focus of the research is the development of the transdermal bandage with desirable properties for the application, low cost, biocompatible and biodegradable.

2. Experimental

2.1 Materials

Soluble potato starch and glycerin (glycerol) by Dinâmica. Polyvinyl alcohol and copper sulfate pentahydrate, by NEON. Nanocrystalline vegetable cellulose (Sodium sulfate cellulose (salt), CAS number: 9005-22-5) by CelluForce. Phosphoric acid, by Synth. Ascorbic acid by Glasslab. Sodium hydroxide in lentils by Merck and ultrapure water (Sartorius Weighing Technology, Germany).

2.2 Methods

2.2.1 Films preparation

Film-forming solutions of 3% m/V potato starch were prepared in water, with a starch:glycerol ratio of 3:1 m/m. It is prepared by constant stirring and heating up to approximately 80°C, to obtain the gelatinization of the material. PVA solubilization solution (concentration of 3% m/m) was carried out under constant stirring and heating at approximately 80°C, until it was completely solubilized.

2.2.2 Films formulations optimization

After preparing the solutions, the TPS and PVA were mixed under stirring for 5 min in the proportions of 60:40, 70:30, 80:20 and 90:10% (m/m), at 80°C. And then, transferred to Petri dishes and taken to the oven for 24 h at 35°C to drying of the films. Based on the methodology used for the preparation of T/P blends (2.2.1), the same procedure was used to produce T/P/CNC films with 2.5; 5.0 and 10.0% (m/m) of CNC by starch mass. In this case, the CNC were previously dispersed in water under sonication for 10 min and then the other components were added during the preparation of the film-forming starch solution.

2.2.3 Preparation of films additive with NPCuO

The same methodology for preparing the T/P/CNC films was used in the production of the films with 0.5% NPCuO (m/m of starch). The choice of a concentration of 0.5% w/w of

NPCuO in the films is based on evidence from the literature demonstrating the effectiveness of different concentrations nanoparticles in similar applications. Manyasree et al. (2017) analyzed concentrations ranging from 0.2% to 0.8%, finding the best results at a concentration of 0.4% [24]. Similarly, Ahmed et al. (2021) identified that the concentration of 0.5% provided the best characteristics in their investigations compared to the use of 0.1% NPCuO [30]. These findings suggest that concentrations between 0.4% and 0.5% of copper oxide nanoparticles are effective in enhancing the desired properties of T/P/CNC films, allowing for the optimization of functional characteristics and potential biomedical applications. Thus, the choice of 0.5% aligns with existing data and can be considered a promising approach to ensure the effectiveness of the films. In this case, the NPCuO were previously dispersed in water under sonication until the solution acquired a greenish and transparent appearance, then the other components were added to prepare the filmogenic solution.

2.2.4 Synthesis and characterization of copper oxide nanoparticles (NPCuO)

2.2.4.1 Synthesis of NPCuO

The synthesis of NPCuO was doing according to the method adapted from *Falconi et.al*, [31], where 20 mL of copper sulfate pentahydrate (7.86 g L^{-1}) were used as metallic precursor. To this solution, 20 mL of ascorbic acid solution (88.1 g L^{-1}) were added dropwise under stirring at 150 rpm, used as stabilizing agent for oxidation and agglomeration, and as reducing agent to the precursor solution, Fig.1.

Then the pH was adjusted to 11 using a sodium hydroxide solution (10.0 g mL^{-1}), dropwise under stirring. After reaching the desired pH, the mixture was heated to 80 ± 1°C, stirring at 150 rpm, for 1 h.

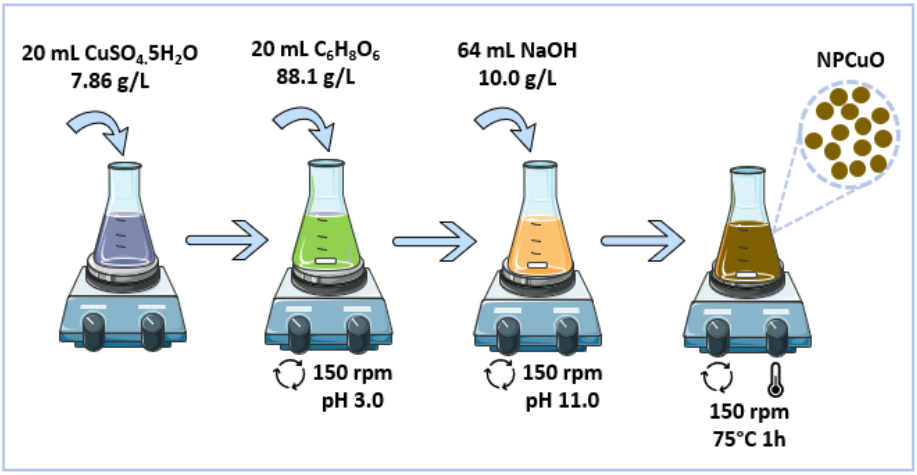

Fig. 1. Representative scheme of the synthesis process of copper oxide nanoparticles (NPCuO).

As an indication of NPCuO formation, it was observed the change in color of the solution to a dark brown color. After reaching room temperature, the solution was centrifuged at 4000 rpm min^{-1} for 15 min. The precipitate formed with NPCuO was collected. For some characterizations, the precipitate was dried for 24 h in an oven at 60°C, to obtain a greenish-black powdery solid.

2.2.4.2 NPCuO characterization

The produced nanoparticles were characterized by UV-Vis, using a Thermo Scientific spectrophotometer, Genesys brand, in aliquots of the final solution containing NPCuO. For measurements, a wavelength range between 500 and 700 nm was used. X-ray diffraction analyzes (XRD) were performed using an Ultima IV - Rigaku model diffractometer, with CuKα radiation (λ=1.54056 Å), Ni filter, 40 kV and 30 mA. X-ray diffractogram was obtained by drying the suspension containing the nanoparticles at 60°C for 24 h until a powder was obtained and analyzed with a 2θ scan from 20 to 80°, with variation of 0.02° and speed of 2° min^{-1}. FTIR measurements were performed using Nicolet Summit equipment, model IR 200, in transmittance mode, using 126.0 scans, nominal resolution of 4.0 cm^{-1}, in the range of 4000 to 400 cm^{-1}. The morphological characterization by scanning electron microscopy (SEM) was carried out in a microscope model TM3000, with an applied acceleration voltage of 20 kV. Peaks ≥ 0.4 cps/eV were considered across the spectrum from 0 to 10 keV. The DLS technique was used to measure the particle size distribution, polydispersity index (PDI) and zeta potential of the particles in suspension. The measurements were carried out on the Zen 1600 Malvern Instruments equipment, with water as the dispersant (RI = 1.330), a viscosity of 0.88 cP, a dielectric constant of 78.5 and a temperature of 25 °C. The analyses were carried out in triplicate. Approximately 10 - 15 measurement cycles of 10 s each were taken and the data obtained was averaged from the respective instrument's pre-loaded software (DTS, version 5.00 from Malvern). The NPCuO were suspended in water at a concentration of 0.01% m/v.

2.3 Films Characterizations

The thickness of the films obtained was determined by using a Mitutoyo digital micrometer (± 0.001 mm) at 10 different points, with the appropriate standard deviation, among all readings. The swelling capacity of the films in the buffer was verified according to the method adapted from *Pal & Pal* [32]. The films were cut into squares (2.0 cm), dried for 2 hours at 70°C and previously weighed, then immersed in 20 mL of phosphate buffer solution

(PBS) at pH 7.0. After each interval (20, 40, 60, 80, 100, 160, 220, 280 e 340 min), the films were dried with absorbent paper and weighed, obtaining wet weight, at 36°C. The procedure and swelling calculation were performed using data in triplicate, through Eq. 1, where: S = Swelling (%), W_w = Wet weight (g), and D_w = Dry weight (g).

$$S(\%) = \frac{Ww-Dw}{Dw}\ x\ 100\% \quad \text{(Eq.1)}$$

The tensile tests were performed in an INSTRON mechanical testing machine, model 4443. The films were cut into strips 15 mm wide and 100 mm long and submitted to a tensile and deformation test at a tensile speed of 10 mm min^{-1}, 250 N load, based on the standard method adapted from ASTM D 882-97 [33]. The results of elongation at break (%) and stress at break (MPa) were obtained. Samples thermal characterization by TGA were carried out in a Perkin Elmer equipment, model Pyris1 TGA. Measurements were performed at a constant heating rate of 10 °C min^{-1} to 700°C, in an inert atmosphere with a flow of 20 mL min^{-1} of nitrogen. The FTIR analysis was performed to verify the composition of the films, in absorbance mode, using 126.0 scans, nominal resolution of 4.0 cm^{-1}, in the range of 4000 to 400 cm^{-1}. The wettability of the films was measured by the sessile drop technique in a Ramé Hart goniometer, model 100-00, with deionized water. For each sample, three drops of water were deposited at different points on the surface, each with 10 contact angle measurements. The results corresponded to the average of the 30 measurements with the standard deviation.

2.4 Qualitative assessment of the optimized films

The films solubility in PBS (pH 7.0) was determined according to the method described by Gontard *et al.*[34], with some modifications. Initially, the films were cut into squares (2.0 cm), the dry matter percentage of the films was determined by weighing, after being kept in an oven at 70°C for 2 h. The films were weighed and immersed in 50 mL of PBS solution and kept under slow stirring at 38°C for 24 h. After this period, each solution was filtered and the retained material was dried in oven at 70°C for 2 h and weighed until constant mass was obtained, thus determining the amount of non-solubilized dry material (Eq. 2). Where: S = Solubility (%), M_i = Initial mass of dry material (g) and M_f = Final mass of non-solubilized dry material (g).

$$S(\%) = \frac{Mi-Mf}{Mi}\ x\ 100\% \quad \text{(Eq. 2)}$$

The permeability was determined gravimetrically according to method E96/E96M-05 [35]. The films were applied in permeation cells (4.5 cm in diameter and 9.0 cm in height) using a silicone ring for fixation. The inside of the cell was partially filled with silica gel (approximately 4 cm high) previously activated in an oven at 200°C. The cells were placed in a desiccator at 25°C and relative humidity of 75% containing distilled water, in which the water vapor permeated through the film was absorbed by the silica. The cell mass was determined daily on analytical balance, making a total of 7 weigh-ins. WVP was calculated according to Eq. 3. Where: WVP = Water Vapor Permeability ($g.mm.m^{-2}.kPa^{-1}.dia^{-1}$), M_{ab} = Mass of absorbed moisture (g), t = Total test time (day), L = Film thickness (mm), A = Film permeation area (m^2).

$$WVP = \frac{Mab}{t}\ x\ \frac{L}{A.\Delta p} \quad \text{(Eq. 3)}$$

2.4.1 Release study of copper oxide nanoparticles

Briefly, the dressings were cut into 2 cm squares with similar masses and placed in PBS buffer solution at 38°C at different time intervals (1-8 h). Then, 3 mL of the solution were removed and placed in a cuvette for measurements at the wavelength of 500 to 750 nm. To quantify the concentration of released nanoparticles, a calibration curve had to be drawn with concentrations of copper nanoparticles from 0.001 to 0.003 g/g of water. The release was evaluated at intervals of 1 h with a maximum duration of 8 h.

2.4.2 Cytotoxicity evaluation

The cytotoxicity of nanocomposites blend (T/P, T/P/10CNC e T/P/10CNC/0,5NPCuO) was studied using 3T3 fibroblast cells. Briefly, cells were grown in adherent culture flasks with Dulbecco's modified Eagle's medium supplemented with 10% fetal calf serum, 0.25 µg ml^{-1} fungizone and 1% penicillin-streptomycin and maintained at 37°C in a humidified chamber (95% air; 5% CO_2) until reaching confluence. To perform the experiments, cells were detached using a trypsin-EDTA solution, stained with trypan blue and counted by a Neubauer camera. To assess cell viability, $2x10^4$ cells were added on top of each sample with 0.5 mL of cell culture medium and maintained at 37°C in a humidified chamber (95% air; 5% CO_2). Cell viability was studied after 24, 48 and 72 hours using the 3-(4,5-dimethyl-thiazol-2-yl)-2,5-diphenyl-tetrazolium bromide (MTT) colorimetric assay. The medium was removed and a 5 mg ml^{-1} MTT solution was added. After incubation for 3 h at 37°C, the MTT solution was

removed, the samples were washed three times with PBS and absolute ethanol was added. Absorbance values were measured at 570 nm and results are expressed as mean ± SD.

2.4.3 Antioxidant Capacity

The DPPH colorimetric assay was conducted to assess the antioxidant capacity of the films. This method relies on measuring the scavenging activity of the 2,2-diphenyl-1-picrylhydrazyl free radical (DPPH•) [36]. In summary, 0.15 g of T/P/10CNC and T/P/10CNC/0.5NPCuO samples were incubated in 3 mL of a methanolic DPPH• solution (25 mg/L) at room temperature. The antioxidant activity was evaluated at 2 hours. Subsequently, the same T/P/10CNC and T/P/10CNC/0.5NPCuO samples were incubated again with a fresh methanolic DPPH• solution, and antioxidant activity was measured at additional intervals of 24, 48, 72, and 96 h, refreshing the DPPH• solution every 24 h. The antioxidant capacity was calculated as a percentage of inhibition using the following equation:

$$\% \text{ inhibition} = [1 - (\text{Abs sample}/\text{Abs DPPH solution})] \times 100 \quad \text{(Eq. 4)}$$

2.5 Statistical Analyses

Based on the data obtained from some analyses, statistical analysis of the numerical results was performed to compare sets of results and verify statistical differences between the studied populations. A one-way ANOVA test, a technique based on variance analysis used to compare the means of several independent populations, was applied. Among the results obtained from the test, the p-value was the parameter used to check for statistically significant differences between the sample sets, with significance established at 5% ($p<0.05$). When values lower than 0.05 were observed for this parameter, a t-test was subsequently performed to verify significant differences between the values for pairs of sample sets.

3. Results and discussions

3.1 Optimization of films formulations

Aiming to improve the properties related to TPS, such as solubility and swelling, PVA was the polymer chosen, based on a review of works in the literature that showed a good synergy between the components [8,10–12,37,38]. Thus, a study of mechanical properties, swelling and thickness was carried out to define the best TPS/PVA ratio. Table 1 shows the results of the study for the different proportions of TPS/PVA.

Table 1. Results of mechanical behavior, in terms of stress and elongation at break, thickness evaluation and swelling in PBS (pH 7.0) for the different TPS/PVA ratios (w/w).

Compositions (TPS/PVA)	Stress at break (MPa)	Elongation at break (%)	Thickness (mm)	Swelling in PBS (%)
0/100	13.4 ± 1.2	212 ± 25	0.061 ± 0.011	#
60/40	4 ± 1.2	32 ± 14*	0.087 ± 0.001	#
70/30	2.5 ± 0.2*	23 ± 9*	0.075 ± 0.005	239 ± 3
80/20	2.1 ± 0.5*	13.11 ± 0.02	0.089 ± 0.004	230 ± 2
90/10	1.5 ± 0.9	7.5 ± 2.2	0.070 ± 0.017	361 ± 4
100/0	0.8 ± 0.1	21.9 ± 2.8	0.078 ± 0.011	39 ± 3

*Samples statistically similar. # Unable to measure (total solubilization). Swelling test conditions: ambient temperature 24.7°C; relative air humidity 46%; samples size 2x2cm; buffer temperature during assay 37.0°C ± 1.0°C.

The results showed significant difference in the values of stress (0.8 MPa) and elongation at break (22%), for the film composed of 100% TPS compared to the other films content TPS, being 13.4 MPa and 212% respectively, close to those found in the literature of 13.5 MPa and 216% for similar films composed exclusively of PVA [39]. For intermediate compositions, the greater the amount of PVA added to the TPS, the greater the toughness of the blends [40]. A material for application as a transdermal dressing needs to be able to adjust to the movements of the region where it will be applied, allowing movement with enough flexibility to not break easily [38].Previous work studying films with potential application in dressings has reported average stress values of 1.71 MPa and average deformation of 27.56% [41] and 1.81 MPa average stress with an average deformation of 26.46% [42], so we can consider the films produced to be within the range observed in the literature for the proposed application. Thickness values were very close to each other, for all films with thicknesses ranging between 0.061 and 0.089 mm. When evaluating the thickness of the films for the intended application, all values obtained were within the range for application as a dressing, which ranges from 0.05 to 0.1 mm [38].

When evaluating the swelling capacity, it was possible to observe that the addition of PVA to TPS improves the swelling capacity of the material. PVA can form hydrogen bonds with the TPS chains, due to the presence of hydroxyl groups in both polymers. These interactions increase the flexibility of the starch matrix by disrupting the strong interactions between the starch chains themselves, making the structure more malleable. In addition, PVA's ability to form hydrogen bonds also facilitates the penetration of water into the matrix, even in small amounts, due to the hydrophilic nature of PVA. For films with higher percentages of PVA in its composition (0/100 and 60/40), it was not possible to calculate a swelling value.

The film composed exclusively of PVA dissolved completely before the first weighing, which was carried out 20 minutes into the test. The 60/40 sample, on the other hand, although not completely solubilized, broke up into small fragments, making the first weighing impossible. Samples 70/30 and 80/20 showed swelling values close to 239 and 230%, respectively, with capacity to absorb more than twice its mass. The best result was obtained with the addition of only 10% PVA, which led to a swelling percentage of 361%, which is a positive result for use in dressings, since it indicates a greater possibility of absorbing the exuded liquid by injuries.

With the addition of small amounts of PVA (10%), hydrogen bonding interactions between the TPS and PVA chains increase the flexibility of the starch matrix, creating sufficient spaces for water penetration. This occurs because PVA helps to disrupt the strong interactions between starch chains, making the structure more malleable and favoring water absorption [43]. As the amount of PVA increases (20% and 30%), interactions between PVA molecules become predominant, resulting in a more compact structure. This compaction reduces the space available for water entry, which in turn decreases the swelling capacity. Furthermore, the high concentration of PVA can lead to a more hydrophilic and unstable matrix, as observed in films with 40% or more PVA, which fragmented or dissolved during the test. Therefore, the 10% PVA proportion represents an ideal balance between matrix flexibility and structural stability, allowing maximum water absorption without compromising the integrity of the film. In the literature, swelling degrees of 100 to 900% have been reported, depending on the material studied [42,44,45], so the value obtained from 361% for the 90/10 sample proved to be suitable for the application.

Thus, the 90/10 (TPS/PVA) composition was chosen to be reinforced with CNC in the subsequent stages, as the optimal ratio for the films due to its high swelling capacity compared to the other compositions analyzed. This behavior is attributed to the higher starch concentration, which is the primary material of interest in this study, given its promising properties such as biocompatibility and biodegradability, as well as its low cost. The elevated swelling capacity makes this formulation particularly attractive for use in transdermal wound dressings, especially for treating wounds that release large amounts of exudate, such as venous ulcers, surgical wounds, and burns [46]. This characteristic allows for greater fluid absorption, maintaining a moist wound environment and promoting the healing process. Furthermore, the predominant use of starch enhances the material's sustainability, aligning with low environmental impact proposals [47]. The results demonstrated the great influence of PVA,

since in addition to its affinity for water, PVA forms hydrogen bonds with the TPS chains, increasing flexibility and facilitating the penetration of water even when added in small amounts [38].

3.1.1 Study of cellulose nanocrystals percentages

Based on the review of literature papers on starch nanocomposites reinforced with cellulose nanocrystals, compositions ranging from 0.25 to 15% of incorporated nanocrystals were reported [48–54]. Thus, the proportions of 2.5, 5.0 and 10.0% of -CNC to be added to 90/10 (TPS/PVA), resulting in nanocomposite blend films. As in the previous stages, studies were carried out regarding mechanical properties, swelling in PBS and thickness, seeking to define which would be the best proportion of CNC to be incorporated, Table 2.

Table 2. Results of the mechanical behavior, in terms of stress and elongation at break, thickness evaluation and swelling in PBS buffer solution (pH 7.0) for the different proportions of CNC (0.0; 2.5; 5.0, 10.0% w/w) incorporated in the 90/10 (T/P) blends.

Compositions (TPS/PVA)	Stress at break (MPa)	Elongation at break (%)	Thickness (mm)	Swelling in PBS (%)
T/P	1.5 ± 0.9	7.5 ± 2.2	0.070 ± 0.017	361 ± 5
T/P/2,5CNC	5.9 ± 1.5	3.9 ± 1.6*	0.093 ± 0.017	295 ± 3.4
T/P/5CNC	8.9 ± 1.4*	3.7 ± 0.7*	0.096 ± 0.006*	265 ± 5
T/P/10CNC	9.1 ± 2.4*	16.5 ± 5.3	0.097 ± 0.016*	249 ± 5

*Samples statistically similar. Swelling test conditions: Ambient temperature 24.7°C. Relative air humidity 46%. Samples size 2x2cm. Buffer temperature during assay 37.0°C ± 1.0°C.

As for the mechanical properties, the results obtained for the stress at break showed that the greater the percentage of reinforcements added, the greater the stress required for film rupture. With the addition of 2.5% CNC (T/P/2.5CNC), the stress at break was approximately 5 times higher compared to the film without reinforcement (T/P), and approximately 10 times higher for the films with 5 and 10% CNC. Statistical analysis showed that there is no statistically significant difference between the T/P/5NCC and T/P/10NCC samples sets in terms of stress measurements at break, indicating that the concentration may be close to the threshold content for this property. The samples with 2.5 and 5.0% (w/w) of CNC, presented a lower percentage of elongation in relation to the 90/10 (T/P) without CNC, and showed no statistically significant difference between them. However the elongation at break doubled for T/P/10CNC, which showed higher elongation values than the other samples with the additivated CNC (16.5 ± 5.3%).

Coelho and his colleagues evaluated the addition of 1, 2, 5, 10 and 15% NCC to TPS matrices in terms of the same mechanical properties investigated in this study. They observed

that the addition of 1 and 2% NCC to the matrix was able to decrease the elongation value in relation to the control starch film, attributing this to the fact that the incorporation of NCC restricts the movement of the starch matrix due to the similarities in chemical structure between the polymeric chains of cellulose and starch which promote strong interactions between their chain segments. However, for the films with the highest incorporation of CNC (5, 10 and 15%), there was a significant increase in tensile strength, because as the amount of NCC increases (5%, 10%, 15%), the material benefits from the reinforcing properties of the cellulose nanocrystals, resulting in a considerable improvement in tensile strength, while the stiffness of the matrix also increases. [52].

The addition of CNC led to an increase in thickness, relative to T/P, which was expected since the nano reinforcements were added at mass percentages of 2.5 to 10% and this greater thickness is due to greater number of solids present in the nanocomposites. The same thickness range was reported in the literature for films with similar compositions [38,52,55].

The addition of 2.5; 5.0 and 10.0% CNC decreased the swelling capacity of the films to 295, 265 and 249%, respectively, The reduction observed in the swelling capacity of all films in relation to the control (T/P – 361%) was attributed to the fact that the introduction of well-dispersed nanocrystals in the hydrophilic T/P matrix induces the formation of intermolecular hydrogen bonds between the components, resulting in the reduced water absorption capacity of the nanocomposite. Similar results have been reported in the literature. Nessi and his collaborators studied TPS/CNC nanocomposites with 1.5, 2.5, 5.0 and 10.0 % nano reinforcements. The swelling capacity for the samples with 1.5 and 2.5% NCC was approximately 130% of the initial mass, while the control sample swelled 150% in relation to the initial mass (NESSI et al., 2019), which supports this hypothesis. However, this effect was lost at a higher NCC content [56,57].

Thus, among the NCC-reinforced samples, the T/P/10CNC composition was chosen to be added to the NPCuO in the next stage of the project. The stress at break increased sixfold with the addition of 10% CNC compared to the unreinforced film. When evaluating the thickness, there was an increase in thickness for this composition compared to the T/P sample, which had the highest value, although this was within the desired range (0.05 to 0.1 mm) for application as a dressing. In addition, all the samples showed the ability of the films to swell, within the desired range for the intended application.

3.2 Synthesis and characterization of copper oxide nanoparticles (NPCuO)

To prove the formation of NPCuO, UV-Vis measurements were performed (Fig.2A), since at the surface of nanometric metallic particles absorbing visible electromagnetic waves, a phenomenon explained through the collective electrons oscillations [58]. UV-Vis spectra revealed absorption at the wavelength of 590 nm for the suspension of nanoparticles, indicating the formation of NPCuO [59].

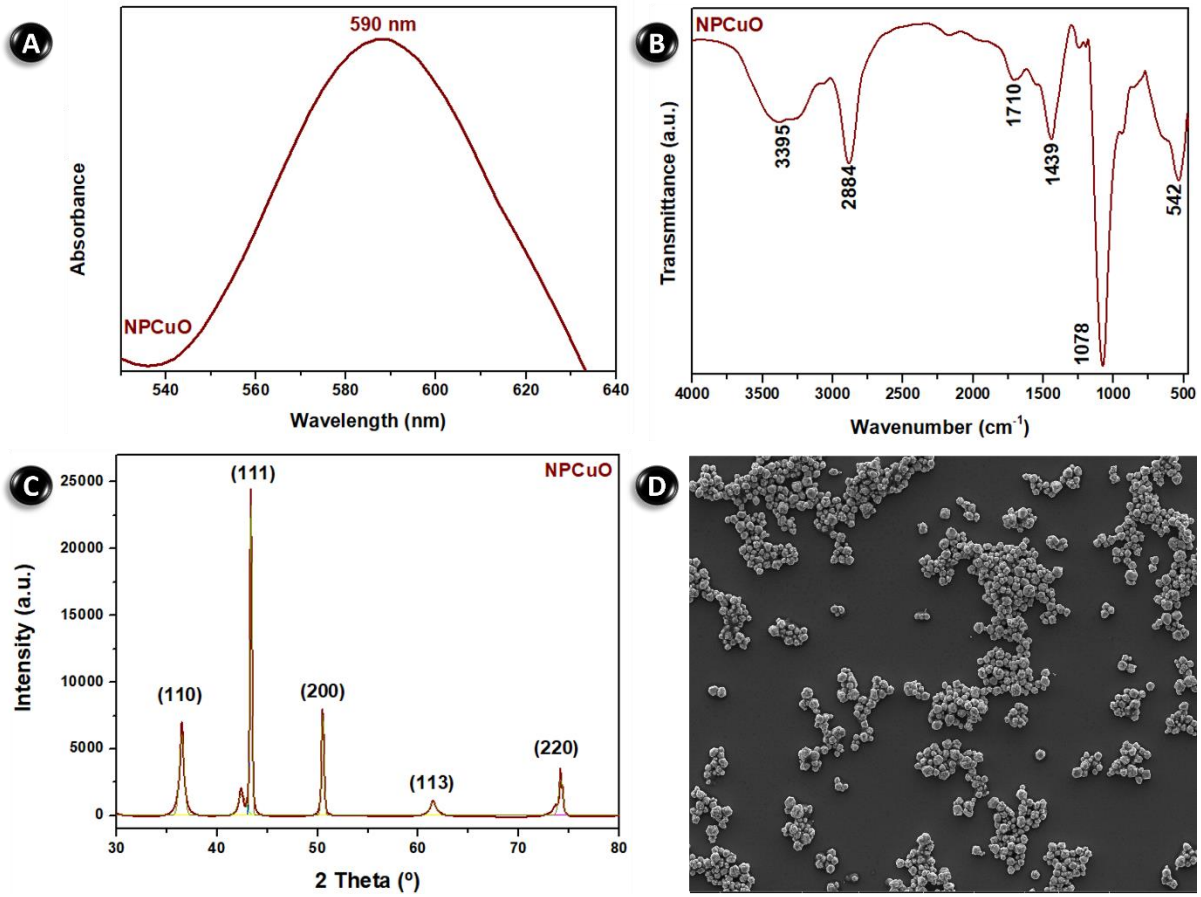

Fig. 2. Analysis of the obtained copper oxide nanoparticles: (A) UV-Vis spectrum; (B) FTIR spectrum; (C) Diffractogram obtained by XRD and (D) Micrograph showing the dispersion of nanoparticles at 2000x magnification.

The FTIR spectrum (Fig.2B) of the dry powder containing NPCuO showed vibrational modes with more expressive signals, characteristic of this type of nanoparticle, as previously reported in the literature. The band centered at 542 cm^{-1} was assigned to the Cu-O stretching vibration [23,24]. Residues of the precursor solution were observed as sulfate ion impurities at 1078 cm^{-1} indicative of the triple degenerative mode, v3, of the SO_4^{-2} ion [24]. At 1439 cm^{-1} the band observed was attributed to a covalent bond between O-H on the surface of CuO [23]. The 2884 cm^{-1} region is characteristic of C-H stretching [60] and the 3395 cm^{-1} is attributed

to the stretching vibration of the water molecule [24], a residue from the drying of the suspension obtained in the synthesis. X-Rays diffractogram (Fig.2C) showed the crystalline nature of the nanoparticles, with the existence of 5 reflection peaks, at 2θ values of 36, 43, 50, 61 and 74°. The characteristic peaks of copper in the metallic form were observed at values of 43°, 50° and 74° and represent, respectively, the Bragg reflections (111), (200) and (220) of the cubic structure of copper [23]. Some of it is copper that has not been oxidized and may be stuck to the particles due to drying. The presented peaks added to 36° and 61°, which represent the reflections (110) and (113), respectively, were similar to those reported in the literature for copper composed nanoparticles and indicate that the crystallites have a face-centered cubic structure [23,24,61].

Micrograph (Fig.2D) obtained from the suspension resulting from the synthesis applied to a silicon wafer by drop-casting, shows a good dispersion of the agglomerates, with heterogeneous distribution, and of different sizes [62]. The average size distribution, PDI and Zeta potential of the NPCuO in suspension were analyzed by DLS. The average size distribution measured for the nanoparticles was 122 ± 3 nm and the value found for the PDI was 0.5 ± 0.2. The average particle size and PDI revealed a high variation in hydrodynamic diameter between the NPCuO in solution. The value found for the average nanoparticle size (122 nm) was slightly smaller than that reported in literature studies, while the PDI of 0.5 was higher than that observed in other studies. The studies reported in the literature resulted in an average size for NPCuO of 148.3 nm with a PDI value of 0.2 [61], 2020), and in another work the average size of NPCuO was 167.1 nm and a polydispersity index of 0.3 [63]. The zeta potential (ζ) of the nanoparticles in suspension was evaluated in triplicate, the result for the NPCuO suspension was -32.8 ± 3.6 mV. The studies also carried out this measurement and found values of -35.3 and -21.00 mV, respectively [61,63]. The data obtained on the surface charges acquired by NPCuO can be used to obtain more information on stability. If all the suspended particles have a positive or negative zeta potential, then they will tend to repel each other, i.e. they will have little tendency to stick together. Particles with zeta potential values more positive than +30 mV or more negative than -30 mV are considered stable [64]. It is important to note that materials with negative surface charges have a longer half-life under biological conditions [65]. Thus, the zeta potential value presented by the NPCuO produced in this work is adequate because it is negative and above the minimum value that guarantees its stability in solution.

3.2.1 Characterizations of NPCuO-additivated films

Based on the review of literature papers, which studied metallic nanoparticles, it was possible to define the concentration of 0.5% [25,29,66–68], in mass of dry NPCuO in relation to the mass of starch used, to be incorporated into the T/P/10CNC composition. Additivated films (T/P/10CNC/0.5NPCuO) were also analyzed regarding the main characteristics for applications. The results obtained in these analyzes were summarized in Table 3.

Table 3. Results of mechanical behavior, in terms of stress and elongation at break, thickness evaluation and swelling in PBS (pH 7.0) for the nanocomposites blend (T/P/10CNC/0.5NPCuO).

Evaluated parameters	T/P/10CNC	T/P/10CNC/0.5NPCuO
Thickness (mm)	0.09 ± 0.01	0.09 ± 0.01
Swelling in PBS (%)	249 ± 5	241 ± 3
Elongation at break (%)	16 ± 5	14 ± 7
Stress at break (MPa)	9 ± 2	9 ± 3

Swelling test conditions: Ambient temperature 24.7°C. Relative air humidity 46%. Samples size 2x2cm. Buffer temperature during assay 37.0°C ± 1.0°C.

The nanocomposite blend showed thickness, swelling capacity in PBS, elongation, and stress at break, as films without addition of nanoparticles (T/P/10CNC). This result was already expected since the added mass was small in relation to the mass of the other components [29,67]. It is worth noting that, regarding swelling, the sample with NPCuO showed a slight reduction in its swelling capacity compared to the non-additivated sample. This can be explained by the fact that the presence of these particles, even in small quantities, reduces the size of the voids between the chains, directly affecting the swelling mechanism of the materials [69].

3.3 Chemical, thermal, and wettability characterization of films

The FTIR spectra obtained for the TPS, PVA, T/P, CNC, T/P/10CNC and T/P/10CNC/0.5NPCuO films are shown in Fig.3A. The 3600 – 3000 cm^{-1} region is typically assigned to hydroxyl bonds, characteristic of hydrogen bonds in the starch D-glucose molecule [70]. With a band centered at 3254 cm^{-1}, characteristic of OH axial deformation, the presence of this band is common to all samples, indicating the contribution of OH stretching, , at 3300 cm^{-1}, which generates changes in the intensity of intermolecular hydrogen bonds in the starch/glycerol system [71].

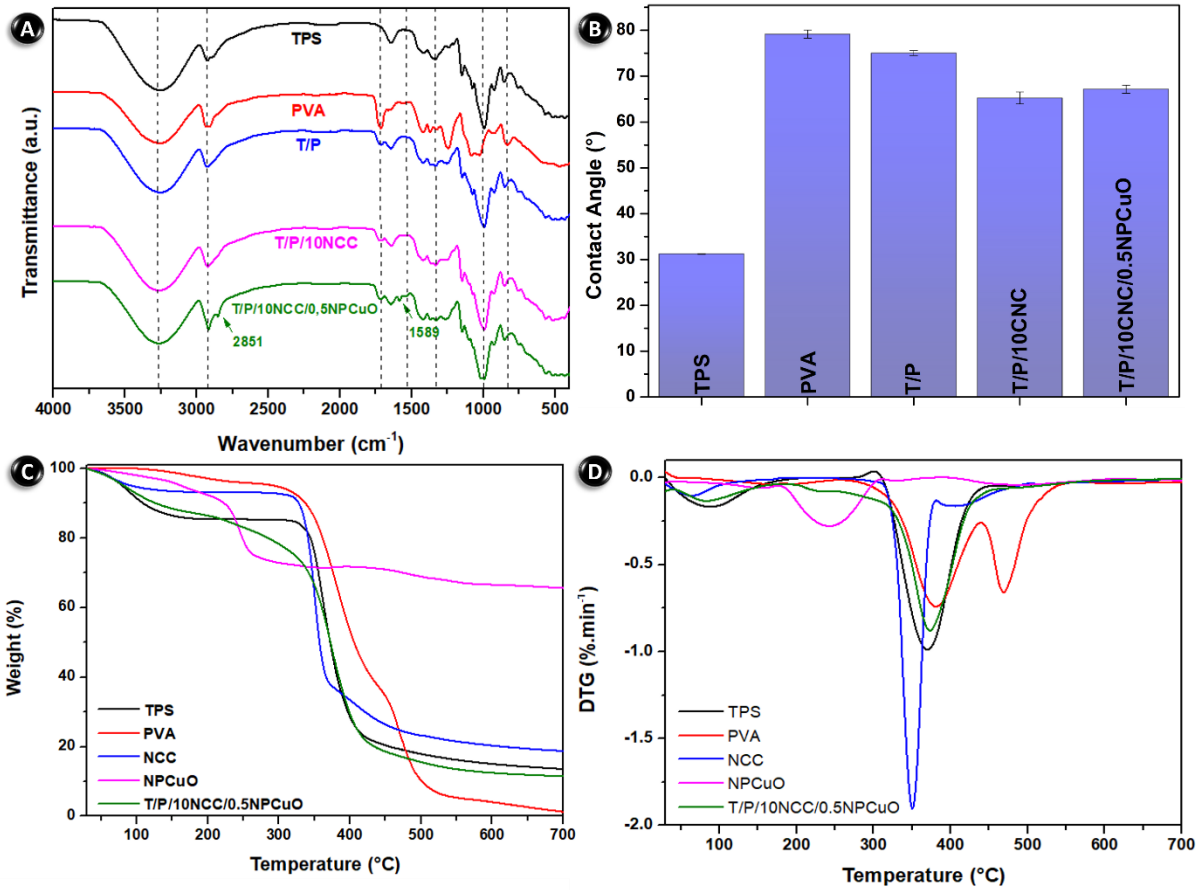

Fig. 3. (A) FTIR spectra obtained for TPS (black), PVA (red), T/P (blue), T/P/10CNC (pink) and T/P/10CNC/0.5NPCuO (green). (B) Contact angle of TPS, PVA, T/P, T/P/10CNC, T/P/10CNC/0.5NPCuO films. (C e D) TG and DTG graphs of TPS (black), PVA (red), T/P (blue), NPCuO (pink) and T/P/10CNC/0.5NPCuO (green), obtained by TGA.

The band centered at 2925 cm^{-1} can be attributed to axial deformation of C-H [72]. There were no significant changes in the region of 2750 - 1750 cm^{-1}. The band centered at 1645 cm^{-1} is characteristic of angular deformation of OH in water and appears only in samples with TPS. The spectrum shows a band at 1540 cm^{-1}, referring to the COO- groups, and another at 1477 cm^{-1}, referring to the COH groups. The band at 1150 cm^{-1} present in TPS spectra is characteristic of the CO group, as well as the one present at 1100 cm^{-1} [73]. At the wavelengths between 1080 and 960 cm^{-1}, characteristic bands of C-O deformation were presented, a region with increased intensity was observed in the TPS spectrum due to the interactions of the plasticizer glycerol and starch. The OH band at 930 cm^{-1} was also be observed, this region is associated with bending or twisting vibrations of the O-H bonds, generally related to more specific interactions between the hydroxyls and other parts of the polymer structure [74]. For PVA, it was possible to observe the band at 1250 cm^{-1} normally associated with CO stretching, and the band near 1750 cm^{-1} may indicate the presence of remaining acetate groups (C=O) [75]. These two bands stand out because the others are very similar to TPS, and are therefore

the most important for identifying PVA in this case. The spectra of the T/P and T/P/10CNC films show no new bands, only overlaps of the characteristic bands of the isolated components. For films with addition of NPCuO, bands were also observed that signal incorporation, one at 2851 and 1589 cm^{-1}, which are characteristic of copper oxide nanoparticles due to a covalent bond between O-H on the surface of CuO [61].

The main films produced were also analyzed for wettability, Fig. 3B. For the TPS film, the contact angle value found was 31.21° ± 0.07°, a result attributed to the hydrophilic character of starch [76], whereas the PVA films showed higher contact angle values (79.1° ± 0.9°). For T/P blend, the angle was 75° ± 5, a result close to that reported in the literature, 77° ± 2° [77]. The increase in the contact angle of the TPS with the formation of the blend with the PVA can be explained by the combination of components in which more hydroxyl groups in the surface layer, both in the TPS and in the PVA molecular chains, interact with each other in the blend, so that there was a connection of the components, making these hydroxyl groups not so available to water [76].With the CNC reinforcement, the angle was reduced to 65° ± 1° (T/P/10CNC), in relation to the T/P composition. It is known that cellulose has a high capacity to interact with water, this is attributed to the high surface area associated with the hydrophilic nature of these reinforcements [78]. For the additive films (T/P/10CNC/0.5NPCuO), the angle was 67° ± 1°, showing an almost inexpressive increase in hydrophobicity. The average value for the contact angle of the studied materials was approximately 62°, showing that in general the films are hydrophilic. This affinity with water is a desirable feature for application as dressings [14].

Through thermogravimetric analysis it was possible to verify the characteristic thermal decomposition of the films using a thermobalance. By analyzing the TPS TG (Fig.3C) and DTG (Fig.3D) curves, it was possible to observe the occurrence of 3 events. The first being the dehydration of the sample occurring from the beginning of the analysis at 30°C to 181°C, with a loss of approximately 14% of water and/or volatile matter, which can also be attributed to the loss of glycerol mass, which has a boiling point at that temperature. The second stage occurred at 181°C and ended at 433°C, attributed to the degradation of potato starch, with a mass loss of 63% [79]. The third stage occurred between approximately 433-700°C, with a mass loss of 8%, and residual formation of 13% of ash attributed to carbonaceous residues [80]. The DTG curve showed two peaks at approximately 84 and 368°C, at these temperatures the rate of mass change in the sample is maximum and were attributed to mass loss of glycerol and starch

respectively. Thus, the TPS degradation stage occurs in two different stages, since the film is composed of 3 parts of starch for one part of glycerol, the percentage of mass loss is compatible in each stage.

When analyzing the PVA, TG and DTG curves (Fig. 3C and D), it was possible to observe the presence of three regions of mass loss, as observed in previous studies [81,82]. The first step between 130 and 239°C can be attributed to the loss of absorbed water molecules, which correspond to a mass loss of approximately 2%, probably due to moisture absorbed by the films. The second stage, occurring between 239 and 415°C, showed a more significant mass loss of about 52%. Part of this loss can be attributed to the release of water more effectively bound to the polymeric matrix [78], indicating a stronger interaction of water with the polymer chains. However, the high value of this mass loss suggests the coexistence of another thermal process. Studies on the thermal degradation of PVA indicate that, in this temperature range, the elimination of side groups from the polymer chains, especially hydroxyl groups (-OH), may occur through intramolecular dehydration reactions. This mechanism leads to the formation of unsaturation (double bonds) in the main chain and the release of water [82]. Water is present in PVA films in different ways, with absorbed molecules, linked by weak bonds, which prefer to be on the external or internal surface without interacting with the matrix, and water molecules strongly linked to hydroxyl groups [81]. The third step between 415 and 515°C was associated with the concomitant degradation process, such as depolymerization, dehydration, destruction of the crystalline part and subsequent formation of carbonized residues decomposition and carbonization of the polymer [83], with a loss of 3% of mass. The residual was approximately 6% by mass.

Analyzing the CNC, TG and DTG curves (Fig. 3C and D), it was possible to distinguish 3 regions of mass loss. The first stage, between 30°C and 106°C, is related to the loss of water adsorbed on the surface of the CNCs, including physically bound water. Additionally, there may be a loss of structural moisture associated with hydroxyl groups present in the cellulose chains, which can interact with water molecules [84]. The mass loss at this stage was relatively low, at 6%. In the second stage, the temperature ranged from 310°C to 383°C, with the main peak on the DTG curve at 350°C. This stage corresponds to the thermal decomposition of the crystalline structure of cellulose, mainly involving the breakdown of glycosidic bonds that link D-glucopyranose units [83]. The decomposition proceeds via pyrolysis, generating carbonaceous products without significant oxidation. This results in a more pronounced mass loss of 65%, due to the decomposition of the polymer backbone, leading to the formation of gaseous products and carbonaceous residues. In the third stage, the temperature ranged between

383°C and approximately 488°C, with a smaller mass loss of around 14%. In this stage, the carbonization of the residues occurs[85], resulting in a higher carbonaceous residue of 19%.

When analyzing the TG and DTG curves for NPCuO, two regions of mass loss can be attributed. The first stage occurred between 30 and 266°C, with a mass loss of 25%. This stage can be attributed to the loss of water adsorbed on the surface of the NPCuO and the decomposition of volatile compounds or organic residues that may be present. Additionally, possible hydroxyl groups bonded to the surface of CuO may be decomposing in this temperature range, contributing to the mass loss. The second stage occurred from 266°C to the final temperature, with a mass loss of 9%. This stage is generally associated with the decomposition of more stable residual compounds formed during synthesis or storage, which decompose, releasing carbon dioxide (CO_2) and leaving CuO as residue. The final residue was high, approximately 33%, and can be attributed to the stable formation of CuO, which is resistant to high temperatures. CuO, being thermally stable, remains the major component of the residue, which is consistent with metal oxide nanoparticles that do not undergo significant decomposition at higher temperatures [86].

The final films were also evaluated, the thermogravimetric curves of the T/P/10CNC/0.5NPCUO film, when analyzing the TG and DTG graphs (Fig.3C and D), it was possible to distinguish two regions of mass loss, the first step between 30 and 126.25°C, corresponding to 9.52% mass loss. Values within this region were observed for the TPS film and the CNC sample, being attributed to the loss of water and/or volatile matter, and the loss of glycerol mass, which has a boiling point at this temperature. The second stage occurred from 126.25 to 457.05 °C, within this region mass loss of TPS, PVA and CNC was observed, which are the main constituents present in the final film, thus being the thermogram in agreement with the thermal behavior of the materials evaluated separately.

3.4 Evaluation of the films for wound dressing applications

The solubility of the films in PBS was evaluated. The results showed that the T/P sample had the lowest solubility, with values close to 11 ± 1%. With the reinforcement of 10% CNC, the solubility of the material increased significantly, jumping to 25 ± 3%, and with the addition of NPCuO to 28 ± 1%, and were considered statistically similar based on the T-Test. An interesting comparative result was observed for the T/P sample, where the swelling content (361%), Table 2, was inversely proportional to the solubility (11%). Indicating that this sample

suffers less solubilization of its components in the medium, which implies a structure capable of swelling more, retaining water in its structure [87].

Reinforcement with 10.0% CNC decreased the swelling capacity of the film (249%) and solubility increased (25%), showing a behavior contrary to the T/P blend. The increase in solubility with the insertion of cellulose reinforcements was attributed to the fact that the introduction of hydrophilic nanocrystals, when well dispersed in the hydrophilic TPS/PVA matrix, led to an increase in hydrophilicity of the material. This result was previously shown in the analysis of the contact angle (Fig. 3C), where the behavior was attributed to the fact that the components used have OH groups in their structures, which allow the formation of hydrogen bonds [87]. This affinity with water is a desirable feature for application as dressings [14].

WVP at an optimized value is a vital parameter to study in a dressing, as it is an indispensable property for wound healing, providing a microenvironment with an ideal moisture level [70]. The results of permeation tests for the different films are shown in Fig.4A. The films show different average WVP values, which were 0.09 $g.mm^{-2}.kPa^{-1}.day^{-1}$ for T/P. With the addition of CNC, the WVP of the films increased to 1.75 $g.mm^{-2}.kPa^{-1}.day^{-1}$ for T/P/10CNC. This behavior was like that previously observed for solubility, which also increased with the addition of nano reinforcements. Probably related to the reduction of intermolecular association via hydrogen and electrostatic interaction in the matrix with the reinforcements that generates a more permeable film [88].

When adding the NPCuO in the film, there was a slight increase in WVP to 1.88 $g.mm^{-2}.kPa^{-1}.day^{-1}$, showing that the nanoparticles could make the films slightly more permeable. Previous works have reported that for normal skin WVP is 0.204 $g.mm^{-2}.day^{-1}$ and for injured skin it is approximately 0.279 to 5.138 $g.mm^{-2}$.day-1, depending on the type of wound [89]. If WVP is too high, complete dehydration of the wound surface can occur, leading to adhesion of the dressing material to the wound surface, decreased body temperature and increased metabolism. In contrast, extremely low permeation values were correlated with exudate accumulation, impaired healing, and increased risk of infection [88]. The literature reports WVP results for commercial dressings, with values from 0.090 to 9.360 $g.mm^{-2}.day^{-1}$ [88,90]. Thus, the result of 1.88 $g.mm^{-2}.kPa^{-1}.day^{-1}$ is within the expected range, which shows the potential for application in commercial dressings.

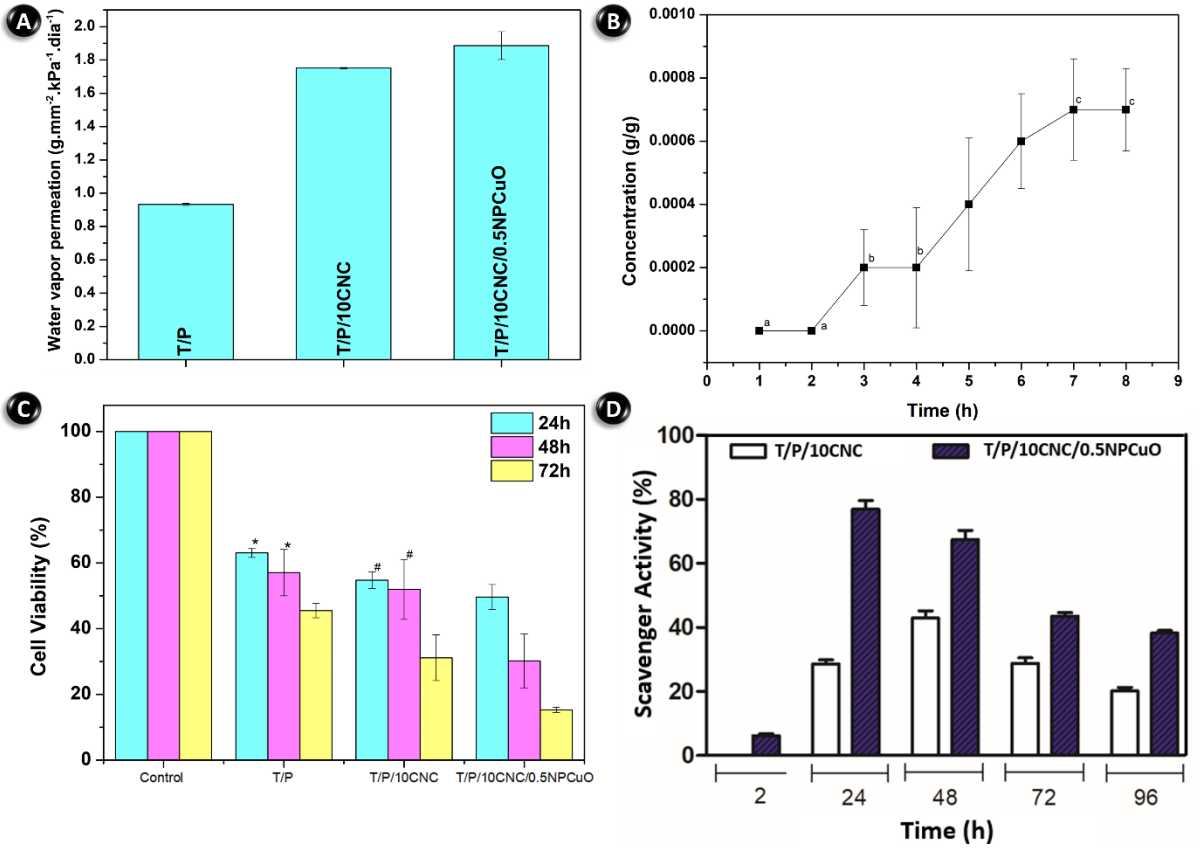

Fig. 4. Results for T/P, T/P/10CNC, and T/P/10CNC/0.5NPCuO films. (A) Water vapor permeation values, monitored for 7 days, expressed in $g.mm^{-2}.kPa^{-1}.day^{-1}$. (B) Results obtained for the release of copper oxide nanoparticles by the nanocomposites, T/P/10CNC/0.5NPCuO at different time intervals, analyzed by UV-Vis spectroscopy. (C) Results of cell viability assay. (D) Antioxidant activity of T/P/10NCC and T/P/10NCC/0.5NPCuO samples, calculated as the % inhibition of DPPH. Results are expressed as mean ± SD from triplicate experiments.

To quantify the concentration of NPCuO released by the film, it was necessary to draw the calibration curve (Absorbance x Concentration) for solutions with known concentrations of NPCuO (0.001 to 0.003 g/g of water). These concentrations were adopted based on the calculated concentration of nanoparticles per gram of film. The release of NPCuO in PBS was monitored to assess the influence of contact time on the release behavior of NPCuO from the film T/P/10CNC/0.5NPCuO. The release measurements were carried out at intervals of 1 hour, up to a maximum of 8 hours, Fig.4B. Based on the measurements, it was possible to observe that the release of NPCuO occurred in a sustained manner [91]. For the T/P/10CNC/0.5NPCuO sample, the first two hours of release were inexpressive (a), but after 3 hours (b) it was possible to observe an increase in the absorption intensity at 590 nm, the wavelength where the maximum absorbance of the nanoparticles occurs [58,59]. In the following hours, the release

occurred progressively until 7 h of study and stagnated at 8 h (c). This behavior was attributed to the film's ability to solubilize in the buffer, which allowed the particles to be released gradually and sustainably [92], and after 8 hours the film was more swollen and solubilized in the medium. The maximum amount of NPCuO released was very low, the calculated concentration of NPCuO present per gram of film was 2 mg and the amount released was 0.7 mg. The retention of the NPCuO can be primarily attributed to the strong chemical affinity between the NPCuO and the hydroxyl groups present in the polymer chains of the film. This interaction can occur through hydrogen bonds and other electrostatic interactions, which keep the nanoparticles firmly bound to the polymeric matrix. As a result, this strong association prevents the release of NPCuO in aqueous media, such as PBS at pH 7, limiting their mobility and increasing retention within the films.[93]

Cell compatibility is a crucial factor to be considered when developing materials for application as transdermal dressings, with the aim of helping wounds to heal without any negative response to the individual who meets this material. For this reason, the cytotoxicity of the samples developed (T/P, T/P/10CNC and T/P/10CNC/0.5NPCuO) and a standard control sample were studied on Madin-Darby Canine Kidney (MDCK) epithelial cells and evaluated using the 3-(4,5-dimethylthiazol-2-yl)-2,5-diphenyl-2H-tetrazolium bromide colorimetric assay (MTT assay). The absorbance values obtained in the MTT test for 24, 48 and 72 hours of the experiment were used to measure the percentage of cell viability of the materials as a function of time, Fig. 4C. The absorbance values obtained in the tests are an indicator of the number of live cells, i.e. the higher the absorbance value, the greater the cell viability of the material. The absorbance values obtained for the control sample were taken as 100% for each test interval. For the T/P sample, a cell viability of approximately 63% was observed during the first 24 hours of the test and approximately 57% after 48 hours, considering the error in the measurements, the viability was maintained (*). After 72 hours there was a slight reduction in cell viability, with values of approximately 45%.

With the addition of CNC (T/P/10CNC), the percentage of viability for 24 and 48 hours of testing was close to 53% (#), which is considered statistically similar, however, after 72 hours there was a significant reduction to 31%. When evaluating the additive sample (T/P/10CNC/0.5NPCuO), cell viability in the first 24 hours was approximately 49%, reduced to 30 and 15% after 48 and 72 hours of testing, respectively. It can thus be concluded that for the T/P and T/P/10CNC samples, cell viability is maintained in the first 48 hours of testing and is reduced after 72 hours. For the T/P/10CNC/0.5NPCuO sample, it is possible to observe a greater reduction in viability between the intervals evaluated, varying from approximately 50%

to 15% between 24 and 72 hours of testing, respectively. However, compared to the control, the cell viability obtained for the developed samples was significantly lower, being less than 70% in all cases, a value considered to be the baseline for cell viability.

Zerboni and his collaborators analyzed the effects of NPZnO and NPCuO on human lung A549 cells and reported a strong cytotoxicity of NPCuO, observing that in 24 h of testing there was a reduction in cell viability evident and that after 48 h almost all the cells evaluated resulted as non-viable for doses of NPCuO ≥10 μg mL^{-1} [94]. This indicates that the added nanoparticles inhibit cell growth probably due to the amount of accumulated copper ions that can be toxic to living epithelial cells, as has been observed in previous work for materials additive with metallic nanoparticles [95,96]. Despite the decrease in cell viability, the number of nanoparticles added can be adjusted to reduce this effect, or it may be convenient to add some other components to increase the cell proliferation of the nanocomposites developed.

The antioxidant activity of the T/P/10CNC and T/P/10CNC/0.5NPCuO films was assessed by measuring the percentage of inhibition of DPPH radical, Fig. 4 D. When comparing T/P/10CNC with T/P/10CNC/0.5NPCuO, we observed that the latter exhibited a faster antioxidant activity over time, achieving a 6.23 ± 0.57% inhibition at 2 hours. These results indicate that the T/P/10CNC/0.5NPCuO film possesses notable antioxidant properties. To further investigate the scavenging activity of both samples over an extended period, we replaced the methanolic DPPH• solution every 24 hours to ensure a continuous supply of the stable radical.

The T/P/10CNC exhibited antioxidant activities of 28.6 ± 1.3% at 24 hours, 43.0 ± 2.3% at 48 hours, 28.8 ± 1.7% at 72 hours, and 20.2 ± 1.2% at 96 hours. In contrast, the T/P/10CNC/0.5NPCuO demonstrated significantly higher antioxidant activities of 76.9 ± 2.8% at 24 hours, 67.4 ± 2.8% at 48 hours, 43.5 ± 1.1% at 72 hours, and 38.2 ± 0.8% at 96 hours. These findings suggest that the T/P/10CNC/0.5NPCuO exhibits superior antioxidant activity compared to T/P/10CNC across all evaluated time points.

In the present study, the amount of NPCuO present per gram of film is approximately 2 mg. For the assay, 0.15 g of film was used in 3 mL of methanolic DPPH• solution, resulting in 0.05 g/mL of film, which corresponds to 0.001 g/mL of NPCuO, or a concentration of 1000 μg/mL of NPCuO. This allows for comparison with other studies in the literature mL [97–99]. The antioxidant activity of NPCuO, based on DPPH radical scavenging activity, has been explored in various studies. Palani *et al.* reported that NPCuO exhibited a DPPH radical scavenging effect of 84.8% at a concentration of 100 μg/mL [97]. Yasin *et al.* investigated the DPPH free radical scavenging ability of NPCuO at varying concentrations. The percentage of

scavenging activity for CuO nanoparticles at concentrations of 0.02, 0.1, 0.5, and 1 mg/mL were 16.5%, 26.866%, 44.8%, and 64.2%, respectively [98]. Ssekataw et al. studied green-synthesized copper oxide nanoparticles (CuONPs) using Camellia sinensis extract (CSE) and Prunus africana bark extract (PAE) at concentrations of 50, 100, 150, 200, 250, and 300 μg/mL. The percentage scavenging activity of the green-synthesized CuONPs increased with concentration and was in line with the plant extracts and the standard. The average values found for CSE-CuONPs were 23.4%, and for PAE-CuONPs, 23.1% [99]. In these studies, there was no variation in assay time, as only a single time point was evaluated.

In comparison to the literature, Palani et al. reported 84.83% DPPH radical scavenging activity for NPCuO at 100 μg/mL, and Yasin et al. showed scavenging activity ranging from 16.5% to 64.2% depending on NPCuO concentration, the T/P/10CNC/0.5NPCuO films in this study demonstrated consistently high antioxidant activity over an extended period. With 76.9% activity at 24 hours and 38.2% at 96 hours, the T/P/10CNC/0.5NPCuO film outperformed many of the green-synthesized CuONPs, which showed lower values around 23% for CSE and PAE extracts. This suggests that the incorporation of NPCuO into the T/P/10CNC matrix enhances its long-term antioxidant capacity compared to standard CuO-based systems.

4. Conclusion

The present study carried out the optimization of the developed film in terms of composition, always focusing on the application. In the study of TPS/PVA proportions, the 90/10% m/m composition stood out among those studied, as it showed the highest swelling capacity in PBS, with values 64% higher than the 80/20 sample, using half the mass of PVA. The results obtained for the 90/10 blend are positive for use in dressings, as they show a greater capacity to absorb exudate from lesions, added to the use of a lower percentage of PVA in its composition, thus reducing the cost of the final material.

Regarding the blend nanocomposites prepared with the addition of CNC, it was possible to observe that the T/P/10CNC composition presented the best results, since the rupture stress was 9 MPa with the addition of 10% CNC, 6 times higher compared to the film without nano reinforcement (1.5 MPa), being the sample with the highest value obtained. Furthermore, the thickness (0.097 mm) and swelling capacity (249%) were within the desired range for the intended application, making it the sample in this set with the greatest application potential.

The average contact angle of the film was approximately 62°, which is a desirable characteristic for applications such as dressings. Regarding solubility in PBS, the samples reinforced with 10% CNC showed a higher percentage of solubility. The WVP of

T/P/10CNC/0.5NPCuO dressings was 1.88 $g.mm^{-2}.kPa^{-1}.day^{-1}$, which is within the range of commercial dressings.

The nanoparticle release studies showed that the maximum amount of NPCuO released was low in relation to the amount added, which can be attributed to the relatively low solubility of the films, around 27%. The T/P/10CNC/0.5NPCuO sample demonstrated significant antioxidant activities with values close to 76% in 24 h, 67% in 48 h, 43% in 72 h and 38% in 96 h, with superior antioxidant activity compared to T/P/10CNC at all points evaluated.

The T/P/10CNC/0.5NPCuO nanocomposite was therefore shown to be a promising material for application as a transdermal dressing, due to its mechanical properties, elongation and tensile strength, swelling capacity and permeability. However, more studies need to be carried out to improve the release capacity of NPCuO and increase cell viability. There is also a need for tests to evaluate the antimicrobial activity of these nanocomposites, which are planned as future activities.

Acknowledgments

This work was financed in part by the Coordination for the Improvement of Higher Education Personnel - Brazil (CAPES) - Financing Code 001. Process Number: 88882.430936/2019- 01 (ASMF) and 88882.427090/2019-01 (JSR). FAPESP projects 2019/15976-0 (APL) and 2020/12659-0 (MF). CNPq grants 308937/2022-8 (APL) and 301955/2019-0 (MF). The authors would like to thank the Servier Medical Art image bank.

References

[1] E. Stasi, A. Giuri, F. Ferrari, V. Armenise, S. Colella, A. Listorti, A. Rizzo, E. Ferraris, C.E. Corcione, Biodegradable carbon-based ashes/maize starch composite films for agricultural applications, Polymers (Basel). 12 (2020) 1–16. https://doi.org/10.3390/polym12030524.

[2] Y. Fan, F. Picchioni, Modification of starch: A review on the application of “green” solvents and controlled functionalization, Carbohydr. Polym. 241 (2020) 116350. https://doi.org/10.1016/j.carbpol.2020.116350.

[3] J. Ren, K.M. Dang, E. Pollet, L. Avérous, Preparation and characterization of thermoplastic potato starch/halloysite nano-biocomposites: Effect of plasticizer nature and nanoclay content, Polymers (Basel). 10 (2018) 15.

https://doi.org/10.3390/polym10080808.

[4] H. Pan, D. Ju, Y. Zhao, Z. Wang, H. Yang, H. Zhang, L. Dong, Mechanical properties, hydrophobic properties and thermal stability of the biodegradable poly(butylene adipate-co-terephthalate)/maleated thermoplastic starch blown films, Fibers Polym. 17 (2016) 1540–1549. https://doi.org/10.1007/s12221-016-6379-x.

[5] J.H.R. Llanos, C.C. Tadini, Preparation and characterization of bio-nanocomposite films based on cassava starch or chitosan, reinforced with montmorillonite or bamboo nanofibers, Int. J. Biol. Macromol. 107 (2018) 371–382. https://doi.org/10.1016/j.ijbiomac.2017.09.001.

[6] N.L. García, L. Famá, N.B. D'Accorso, S. Goyanes, Biodegradable Starch Nanocomposites, in: V.K. Thakur, M.K. Thakur (Eds.), Eco-Friendly Polym. Nanocomposites Process. Prop., Springer India, New Delhi, 2015: pp. 17–77. https://doi.org/10.1007/978-81-322-2470-9.

[7] H. Liu, F. Xie, L. Yu, L. Chen, L. Li, Thermal processing of starch-based polymers, Prog. Polym. Sci. 34 (2009) 1348–1368. https://doi.org/10.1016/j.progpolymsci.2009.07.001.

[8] X. Lin, N. Li, Q. Xiao, Y. Guo, J. Wei, T. Jiao, Q. Chen, Q. Chen, X. Chen, Polyvinyl alcohol/starch-based film incorporated with grape skin anthocyanins and metal-organic framework crystals for colorimetric monitoring of pork freshness, Food Chem. 395 (2022) 133613. https://doi.org/10.1016/J.FOODCHEM.2022.133613.

[9] F.C. Britto, D.C. Olsson, J.L. Ampessan, G.T. Zanella, P.H.M. Kehl, M.L. Oldoni, R. Kramer, N. Fronza, Desenvolvimento de biofilme à base de amido para aplicação em sistema transdérmico, in: An. Da IV MIC - Most. Iniciação Científica Do IFC - Inst. Fed. Catarinense - Câmpus Concórdia, 2014.

[10] J. Yu, D. Wei, S. Li, Q. Tang, H. Li, Z. Zhang, W. Hu, Z. Zou, High-performance multifunctional polyvinyl alcohol/starch based active packaging films compatibilized with bioinspired polydopamine nanoparticles, Int. J. Biol. Macromol. 210 (2022) 654–662. https://doi.org/10.1016/J.IJBIOMAC.2022.04.221.

[11] J. Porras-Saavedra, L. Ricaurte, N.C. Pérez-Pérez, M.X. Quintanilla-Carvajal, Development and characterization of Sechium edule starch and polyvinyl alcohol nanofibers obtained by electrospinning, Colloids Surfaces A Physicochem. Eng. Asp. 649 (2022) 129456. https://doi.org/10.1016/J.COLSURFA.2022.129456.

[12] P. Punnoy, P. Preechakasedkit, C. Aumnate, N. Rodthongkum, P. Potiyaraj, N. Ruecha, Polyvinyl alcohol/starch modified cotton thread surface as a novel

colorimetric glucose sensor, Mater. Lett. 299 (2021) 130076. https://doi.org/10.1016/J.MATLET.2021.130076.

[13] T.L. do A. Montanheiro, L.S. Montagna, V. Patrulea, O. Jordan, G. Borchard, G.M.M. Lobato, L.H. Catalani, A.P. Lemes, Evaluation of cellulose nanocrystal addition on morphology, compression modulus and cytotoxicity of poly(3-hydroxybutyrate-co-3-hydroxyvalerate) scaffolds, J. Mater. Sci. 54 (2019) 7198–7210. https://doi.org/10.1007/s10853-019-03398-8.

[14] J.B. et al Rodrigues, SÍNTESE DE HIDROGÉIS DE AMIDO/NANOPARTÍCULAS DE PRATA PARA APLICAÇÃO COMO CURATIVO, in: 9° Congr. Latino-Americano Orgãos Artif. e Biomateriais, 2016: p. 2016.

[15] H. Dai, S. Ou, Y. Huang, H. Huang, Utilization of pineapple peel for production of nanocellulose and film application, Cellulose. 25 (2018) 1743–1756. https://doi.org/10.1007/s10570-018-1671-0.

[16] D.C. Olsson, G. Schiochet, J. Ampessan, K. Rossi, R. Albrecht, F. Vieira, G.M. Locatelli, C.L. Albring, M. Gabriel, C. Schwertz, R.E. Mendes, N. Fronza, A. Vargas Junior, Avaliação Da Resposta Cicatricial À Aplicação Dérmica De Scaffold a Base De Amido Aditivado Em Feridas Cirúrgicas De Oryctolagus Cuniculus Em Modelo Experimental, Rev. Ciência Veterinária e Saúde Pública. 5 (2018) 025. https://doi.org/10.4025/revcivet.v5i1.37735.

[17] F. Jiang, Y. Lo Hsieh, Cellulose nanocrystal isolation from tomato peels and assembled nanofibers, Carbohydr. Polym. 122 (2015) 60–68. https://doi.org/10.1016/j.carbpol.2014.12.064.

[18] S. Naz, N. Ahmad, J. Akhtar, N.M. Ahmad, A. Ali, M. Zia, Management of citrus waste by switching in the production of nanocellulose, IET Nanobiotechnology. 10 (2016) 395–399. https://doi.org/10.1049/iet-nbt.2015.0116.

[19] A.Y. Melikoğlu, S.E. Bilek, S. Cesur, Optimum alkaline treatment parameters for the extraction of cellulose and production of cellulose nanocrystals from apple pomace, Carbohydr. Polym. 215 (2019) 330–337. https://doi.org/10.1016/j.carbpol.2019.03.103.

[20] G. Siaueira, J. Bras, A. Dufresne, Cellulose whiskers versus microfibrils: Influence of the nature of the nanoparticle and its surface functionalization on the thermal and mechanical properties of nanocomposites, Biomacromolecules. 10 (2009) 425–432. https://doi.org/10.1021/bm801193d.

[21] Z.W. Abdullah, Y. Dong, Recent advances and perspectives on starch nanocomposites

for packaging applications, J. Mater. Sci. 53 (2018) 15319–15339. https://doi.org/10.1007/s10853-018-2613-9.

[22] S. Forouzandehdel, S. Forouzandehdel, M. Rezghi Rami, Synthesis of a novel magnetic starch-alginic acid-based biomaterial for drug delivery, Carbohydr. Res. 487 (2020) 107889. https://doi.org/10.1016/j.carres.2019.107889.

[23] A.R. Maheo, S.M.V. B., A.A.P. T., Biosynthesis and characterization of Eupatorium adenophorum and chitosan mediated Copper oxide nanoparticles and their antibacterial activity, Results in Surfaces and Interfaces. 6 (2022) 100048. https://doi.org/10.1016/j.rsurfi.2022.100048.

[24] D. Manyasree, K.M. Peddi, R. Ravikumar, CuO nanoparticles: Synthesis, characterization and their bactericidal efficacy, Int. J. Appl. Pharm. 9 (2017) 71–74. https://doi.org/10.22159/ijap.2017v9i6.71757.

[25] O. V. López, M.E. Villanueva, G.J. Copello, M.A. Villar, Flexible thermoplastic starch films functionalized with copper particles for packaging of food products, Funct. Compos. Mater. 1 (2020) 1–17. https://doi.org/10.1186/s42252-020-00009-7.

[26] E. Arezoo, E. Mohammadreza, M. Maryam, M.N. Abdorreza, The synergistic effects of cinnamon essential oil and nano TiO2 on antimicrobial and functional properties of sago starch films, Int. J. Biol. Macromol. 157 (2020) 743–751. https://doi.org/10.1016/j.ijbiomac.2019.11.244.

[27] F. Ortega, L. Giannuzzi, V.B. Arce, M.A. García, Active composite starch films containing green synthetized silver nanoparticles, Food Hydrocoll. 70 (2017) 152–162. https://doi.org/10.1016/j.foodhyd.2017.03.036.

[28] H. Glycerol, E. Films, How Glycerol and Water Contents Affect the Structural and Functional Properties of Starch-Based, (2018). https://doi.org/10.3390/polym10040412.

[29] M.S. Mohseni, M.A. Khalilzadeh, M. Mohseni, F.Z. Hargalani, M.I. Getso, V. Raissi, O. Raiesi, Green synthesis of Ag nanoparticles from pomegranate seeds extract and synthesis of Ag-Starch nanocomposite and characterization of mechanical properties of the films, Biocatal. Agric. Biotechnol. 25 (2020) 101569. https://doi.org/10.1016/j.bcab.2020.101569.

[30] S.B. Ahmed, H.I. Mohamed, A.M. Al-Subaie, A.I. Al-Ohali, N.M.R. Mahmoud, Investigation of the antimicrobial activity and hematological pattern of nano-chitosan and its nano-copper composite, Sci. Rep. 11 (2021) 1–9. https://doi.org/10.1038/s41598-021-88907-z.

[31] ALVES I.F.B, MARTINS T.A.G, BALTAZAR M.DOS P.G, DE MORAES V.T., ESPINOSA D.C.R, TENÓRIO, Síntese De Nanopartículas De Cobre Para Aplicação No Processo Oxidativo Foto- Fenton Para a Degradação De Surfactantes, (2019).

[32] K. Pal, S. Pal, Development of porous hydroxyapatite scaffolds, Mater. Manuf. Process. 21 (2006) 325–328. https://doi.org/10.1080/10426910500464826.

[33] American Society for Testing and Materials. ASTM., Standard test methods for tensile properties of thin plastic sheeting, method D882-10., Annu. B. ASTM Stand. 87 (2010) 3–5. https://doi.org/10.1520/D0882-10.2.

[34] N. GONTARD, S. GUILBERT, J. -L CUQ, Edible Wheat Gluten Films: Influence of the Main Process Variables on Film Properties using Response Surface Methodology, J. Food Sci. 57 (1992) 190–195. https://doi.org/10.1111/j.1365-2621.1992.tb05453.x.

[35] ASTM, Standard Test Methods for Water Vapor Transmission of Shipping Containers —, Am. Soc. Test. Mater. 95 (2003) 4–6. https://doi.org/10.1520/E0096.

[36] P.E. Antezana, S. Municoy, G. Orive, M.F. Desimone, Design of a New 3D Gelatin—Alginate Scaffold Loaded with Cannabis sativa Oil, Polymers (Basel). 14 (2022). https://doi.org/10.3390/polym14214506.

[37] W.P.S. Rodrigues, J.V.V. Ribeiro, C.R.B. da Silva, I.T.N. de Campos, C.H. Xavier, F.C.A. dos Santos, M. V. Cruz, K.F. Fernandes, In vivo effect of orally given polyvinyl alcohol/starch nanocomposites containing bioactive peptides from Phaseolus vulgaris beans, Colloids Surfaces B Biointerfaces. 209 (2022) 112213. https://doi.org/10.1016/J.COLSURFB.2021.112213.

[38] P.L. da Silva, A.M.M. Gomes, N.M.P.S. Ricardo, T.F. Machado, ELABORAÇÃO E CARACTERIZAÇÃO DE BLENDAS DE AMIDO FOSFORILADO COM QUITOSANA E PVA, Quim. Nova. 39 (2016) 450–455. https://doi.org/http://dx.doi.org/10.5935/0100-4042.20160043.

[39] G. Kavoosi, B. Nateghpoor, S.M.M. Dadfar, S.M.A. Dadfar, Antioxidant, antifungal, water binding, and mechanical properties of poly(vinyl alcohol) film incorporated with essential oil as a potential wound dressing material, J. Appl. Polym. Sci. 131 (2014) 1–8. https://doi.org/10.1002/app.40937.

[40] G.D. Mogoşanu, A.M. Grumezescu, Natural and synthetic polymers for wounds and burns dressing, Int. J. Pharm. 463 (2014) 127–136. https://doi.org/10.1016/j.ijpharm.2013.12.015.

[41] B.P. Antunes, A.F. Moreira, V.M. Gaspar, I.J. Correia, Chitosan/arginine-chitosan polymer blends for assembly of nanofibrous membranes for wound regeneration,

Carbohydr. Polym. 130 (2015) 104–112. https://doi.org/10.1016/j.carbpol.2015.04.072.

[42] R.S. Novak, R. Letícia, J.T. Espinoza, J. De, F.P. De Paula, D.P. Ciências, U. Estadual, D.P. Grossa, C. Alunos, C. De Pós-graduação, C. Farmacêuticas, U.E. De, OPEN ACCESS VERDE , A PARTIR DO EXTRATO AQUOSO DE GENGIBRE, 11 (2021) 45685–45692.

[43] A.G.V. de C. Neto, D.I. Dos Santos, S.R. Rissato, M.J. Saeki, S.L. Favaro, E. Radovanovic, D.S. Pellosi, Evaluation of the physical, chemical and mechanical properties of starch/PVA/bentonite clay films modified with glycidyl methacrylate, Rev. Mater. 25 (2020) 1–15. https://doi.org/10.1590/s1517-707620200003.1135.

[44] W.C. Lin, C.C. Lien, H.J. Yeh, C.M. Yu, S.H. Hsu, Bacterial cellulose and bacterial cellulose-chitosan membranes for wound dressing applications, Carbohydr. Polym. 94 (2013) 603–611. https://doi.org/10.1016/j.carbpol.2013.01.076.

[45] P.I. Morgado, A. Aguiar-Ricardo, I.J. Correia, Asymmetric membranes as ideal wound dressings: An overview on production methods, structure, properties and performance relationship, J. Memb. Sci. 490 (2015) 139–151. https://doi.org/10.1016/j.memsci.2015.04.064.

[46] M.M. Delavari, I. Ocampo, I. Stiharu, Optimizing Biodegradable Starch-Based Composite Films Formulation for Wound-Dressing Applications, Micromachines. 13 (2022). https://doi.org/10.3390/mi13122146.

[47] M.M. Delavari, I. Stiharu, Preparing and Characterizing Novel Biodegradable Starch/PVA-Based Films with Nano-Sized Zinc-Oxide Particles for Wound-Dressing Applications, Appl. Sci. 12 (2022). https://doi.org/10.3390/app12084001.

[48] K. González, O. Guaresti, T. Palomares, A. Alonso-Varona, A. Eceiza, N. Gabilondo, The role of cellulose nanocrystals in biocompatible starch-based clicked nanocomposite hydrogels, Int. J. Biol. Macromol. 143 (2020) 265–272. https://doi.org/10.1016/j.ijbiomac.2019.12.050.

[49] J. Li, M. Zhou, G. Cheng, F. Cheng, Y. Lin, P.X. Zhu, Fabrication and characterization of starch-based nanocomposites reinforced with montmorillonite and cellulose nanofibers, Carbohydr. Polym. 210 (2019) 429–436. https://doi.org/10.1016/j.carbpol.2019.01.051.

[50] J.C. Cerqueira, J. Da Silva Penha, R.S. Oliveira, L.L. Nani Guarieiro, P. Da Silva Melo, J.D. Viana, B.A. Souza Machado, Production of biodegradable starch nanocomposites using cellulose nanocrystals extracted from coconut fibers, Polimeros.

27 (2017) 320–329. https://doi.org/10.1590/0104-1428.05316.

[51] K. Xu, C. Liu, K. Kang, Z. Zheng, S. Wang, Z. Tang, W. Yang, Isolation of nanocrystalline cellulose from rice straw and preparation of its biocomposites with chitosan: Physicochemical characterization and evaluation of interfacial compatibility, Compos. Sci. Technol. 154 (2018) 8–17. https://doi.org/10.1016/j.compscitech.2017.10.022.

[52] C.C. de S. Coelho, R.B.S. Silva, C.W.P. Carvalho, A.L. Rossi, J.A. Teixeira, O. Freitas-Silva, L.M.C. Cabral, Cellulose nanocrystals from grape pomace and their use for the development of starch-based nanocomposite films, Int. J. Biol. Macromol. 159 (2020) 1048–1061. https://doi.org/10.1016/j.ijbiomac.2020.05.046.

[53] B. Montero, M. Rico, S. Rodríguez-Llamazares, L. Barral, R. Bouza, Effect of nanocellulose as a filler on biodegradable thermoplastic starch films from tuber, cereal and legume, Carbohydr. Polym. 157 (2017) 1094–1104. https://doi.org/10.1016/j.carbpol.2016.10.073.

[54] A. Olad, F. Doustdar, H. Gharekhani, Fabrication and characterization of a starch-based superabsorbent hydrogel composite reinforced with cellulose nanocrystals from potato peel waste, Colloids Surfaces A Physicochem. Eng. Asp. 601 (2020) 124962. https://doi.org/10.1016/j.colsurfa.2020.124962.

[55] B.A.S. Machado, I.L. Nunes, F.V. Pereira, J.I. Druzian, Desenvolvimento e avaliação da eficácia de filmes biodegradáveis de amido de mandioca com nanocelulose como reforço e com extrato de erva-mate como aditivo antioxidante, Cienc. Rural. 42 (2012) 2085–2091. https://doi.org/10.1590/S0103-84782012001100028.

[56] V. Nessi, X. Falourd, J.E. Maigret, K. Cahier, A. D'Orlando, N. Descamps, V. Gaucher, C. Chevigny, D. Lourdin, Cellulose nanocrystals-starch nanocomposites produced by extrusion: Structure and behavior in physiological conditions, Carbohydr. Polym. 225 (2019). https://doi.org/10.1016/j.carbpol.2019.115123.

[57] M.C. Popescu, Structure and sorption properties of CNC reinforced PVA films, Int. J. Biol. Macromol. 101 (2017) 783–790. https://doi.org/10.1016/j.ijbiomac.2017.03.168.

[58] N. Begletsova, E. Selifonova, A. Chumakov, A. Al-Alwani, A. Zakharevich, R. Chernova, E. Glukhovskoy, Chemical synthesis of copper nanoparticles in aqueous solutions in the presence of anionic surfactant sodium dodecyl sulfate, Colloids Surfaces A Physicochem. Eng. Asp. 552 (2018) 75–80. https://doi.org/10.1016/j.colsurfa.2018.05.023.

[59] S. Pradhan, Green Synthesis of Copper Nanoparticles Using Aloe Vera and Its

characterization, Int. J. Inf. Res. Rev. 05 (2018) 5410–5414.

[60] H. Mahmoudvand, M. Khaksarian, K. Ebrahimi, S. Shiravand, Antinociceptive e ff ects of green synthesized copper nanoparticles alone or in combination with morphine, Ann. Med. Surg. 51 (2020) 31–36. https://doi.org/10.1016/j.amsu.2019.12.006.

[61] A.V.A. Mariadoss, K. Saravanakumar, A. Sathiyaseelan, K. Venkatachalam, M.H. Wang, Folic acid functionalized starch encapsulated green synthesized copper oxide nanoparticles for targeted drug delivery in breast cancer therapy, Int. J. Biol. Macromol. 164 (2020) 2073–2084. https://doi.org/10.1016/j.ijbiomac.2020.08.036.

[62] K.L.A.P. M. Rashad; M. Rüsing; G. Berth, CuO and Co3O4 Nanoparticles: Synthesis, Characterizations, and Raman Spectroscopy, Phys. Chem. Chem. Phys. 18 (2015) 926–931. http://dx.doi.org/10.1039/C5CP06815K.

[63] S. Vinitha, J. Vijayalakshmi, S.T. Johny, A.J. Margenot, D.A. Rippner, M.R. Dumlao, S. Nezami, P.G. Green, S.J. Parikh, A.J. Mcelrone, G.M. Sulaiman, R. Chowdhury, A.A. Khan, H. Rashid, J. Santhoshkumar, V. Shanmugam, O. Nanoparticles, F. Amin, B. Khattak, A. Alotaibi, M. Qasim, I. Ahmad, R. Ullah, M. Bourhia, A.A. Gul, S. Zahoor, R. Ahmad, N. Rabiee, M. Bagherzadeh, M. Kiani, A.M. Ghadiri, F. Etessamifar, A.H. Jaberizadeh, A. Shakeri, I. Hasan, P. Singh, M. Batool, Z. Qureshi, F. Hashmi, N. Mehboob, S.N. Begum, A. Esakkiraja, S.M. Asan, M. Muthumari, G.V. Raj, S. Kanagasubbulakshmi, K. Kadirvelu, K. Gebremedhn, M.H. Kahsay, M. Aklilu, S. Sukumar, A. Rudrasenan, D.P. Nambiar, I.J.A. Res, S. Fatma, P. Kalainila, E. Ravindran, S. Renganathan, M. Altikatoglu, A. Attar, F. Erci, C.M. Cristache, I. Isildak, S. Jayakodi, T. Nadu, F. Ijaz, S. Shahid, S.A. Khan, W. Ahmad, W.W. Andualem, F.K. Sabir, E.T. Mohammed, H.H. Belay, B.A. Gonfa, H. Le Tu, D.D. Gultekin, H. Nadaroglu, K. Nomura, P. Terwilliger, D. Berra, S.E. Laouini, B. Benhaoua, M.R. Ouahrani, D. Berrani, A. Rahal, E.H. Lakhdar, S.M. Yedurkar, C.B. Maurya, P.A. Mahanwar, K.S. Shiny, R. Sundararaj, N. Mamatha, B. Lingappa, S. Raj, R. Trivedi, K. Ganesan, V. Kumar, A. Natarajan, A. Rajaram, S. Ravichandran, S. Ramalingam, D. Letchumanan, S.P.M. Sok, S. Ibrahim, N.H. Nagoor, N.M. Arshad, K.S. Shiny, R. Sundararaj, A. Jayadev, N.K. B, A.M. Al-fa, M.H. Abu-kharma, A.M. Awwad, R. Radhakrishnan, F. Liakath, A.A. Khan, A. Muthu, V. Balakrishnan, K. Thangaraj, M. Palani, M.W. Shammout, A.M. Awwad, H. Veisi, B. Karmakar, T. Tamoradi, S. Hemmati, M. Hekmati, R. Lett, M. Ali, M. Ijaz, M. Ikram, A.U. Hamid, M. Avais, A.A. Anjum, S. Paul, A. Sheyi, I.D. Bangu, S.I. Abubakar, M. Muazu, P.G. Bhavyasree, T.S. Xavier, A. You, M.A.Y. Be, I. In, H.C.A. Murthy, B. Abebe, T.D. Z,

J. Sarkar, N. Chakraborty, A. Chatterjee, A. Bhattacharjee, M. Mohamed, I.H. Ibrahim, N. Raafat, H.I. Mohamed, A.M. Sallam, E.A. Mohamed, S. Drummer, T. Madzimbamuto, M. Chowdhury, S. Naz, A.A. Gul, M. Zia, R.D. Widyastuti, S. Susanto, A. Idris, A.C. Linatoc, C. Hidayat, Review Article Synthesis of CuO Nanoparticles Using Aloe Vera Leaf Extract and its Cytotoxic Effects on Human Carcinoma Cells, Curr. Res. Green Sustain. Chem. 5 (2020) 1–8. https://doi.org/10.1016/j.heliyon.2019.e03123%0Ahttps://doi.org/10.1016/j.crgsc.2021.100249%0Ahttps://doi.org/10.1186/s11671-021-03605-z%0Ahttps://doi.org/10.1038/s41598-021-81320-6%0Ahttps://doi.org/10.1080/24701556.2021.1952260%0Ahttps://doi.org/10.1016.

[64] S. Bhatnagar, T. Kobori, D. Ganesh, K. Ogawa, H. Aoyagi, Biosynthesis of silver nanoparticles mediated by extracellular pigment from talaromyces purpurogenus and their biomedical applications, Nanomaterials. 9 (2019) 1–27. https://doi.org/10.3390/nano9071042.

[65] A.C.S.L. MONICI, PRODUÇÃO, OTIMIZAÇÃO E CARACTERIZAÇÃO DE NANOPARTÍCULAS DE SILICATOS PARA O TRANSPORTE DE COMPOSTOS DE INTERESSE TERAPÊUTICO, Universidade de Brasília, 2020.

[66] X. Hu, X. Jia, C. Zhi, Z. Jin, M. Miao, Improving the properties of starch-based antimicrobial composite films using ZnO-chitosan nanoparticles, Carbohydr. Polym. 210 (2019) 204–209. https://doi.org/10.1016/j.carbpol.2019.01.043.

[67] Y. Xu, N. Rehmani, L. Alsubaie, C. Kim, E. Sismour, A. Scales, Tapioca starch active nanocomposite films and their antimicrobial effectiveness on ready-to-eat chicken meat, Food Packag. Shelf Life. 16 (2018) 86–91. https://doi.org/10.1016/j.fpsl.2018.02.006.

[68] M.A.G. Florencia Ortega, Leda Giannuzzi, Valeria B. Arce, Active composite starch films containing green synthetized silver nanoparticles, Carbohydr. Polym. 169 (2020) 1–17. https://doi.org/10.1016/j.postharvbio.2017.03.005.

[69] M.R. Fischer, M.C.F. Garcia, A.L. Nogueira, L.M. Porto, A.L. dos S. Schneider, A.P.T. Pezzin, Biossíntese e caracterização de nanocelulose bacteriana para engenharia de tecidos, Rev. Mater. 22 (2017). https://doi.org/10.1590/s1517-707620170005.0270.

[70] N. Wang, X. Zhang, N. Han, S. Bai, Effect of citric acid and processing on the performance of thermoplastic starch/montmorillonite nanocomposites, Carbohydr. Polym. 76 (2009) 68–73. https://doi.org/10.1016/j.carbpol.2008.09.021.

[71] X. Ma, J. Yu, The effects of plasticizers containing amide groups on the properties of

thermoplastic starch, Starch/Staerke. 56 (2004) 545–551. https://doi.org/10.1002/star.200300256.

[72] H.A. Pyshpadass, D.B. Marx, M.A. Hanna, Effects of extrusion temperature and plasticizers on the physical and functional properties of starch films, Starch/Staerke. 60 (2008) 527–538. https://doi.org/10.1002/star.200800713.

[73] N. Saifuddin, H. Refal, P. Kumaran, Rapid purification of glycerol by-product from biodiesel production through combined process of microwave assisted acidification and adsorption via chitosan immobilized with yeast, Res. J. Appl. Sci. Eng. Technol. 7 (2014) 593–602. https://doi.org/10.19026/rjaset.7.295.

[74] K.C. Reis, J. Pereira, A.C. Smith, C.W.P. Carvalho, N. Wellner, I. Yakimets, Characterization of polyhydroxybutyrate-hydroxyvalerate (PHB-HV)/maize starch blend films, J. Food Eng. 89 (2008) 361–369. https://doi.org/10.1016/j.jfoodeng.2008.04.022.

[75] M.M. Atta, A.M. Abdel Reheem, Effect of nitrogen ions on the structural, optical, and thermal properties of polyvinyl alcohol/starch blend, Curr. Appl. Phys. 36 (2022) 43–50. https://doi.org/10.1016/J.CAP.2021.11.016.

[76] C.L. Luchese, P. Benelli, J.C. Spada, I.C. Tessaro, Impact of the starch source on the physicochemical properties and biodegradability of different starch-based films, J. Appl. Polym. Sci. 135 (2018) 1–11. https://doi.org/10.1002/app.46564.

[77] J. Zhou, Y. Ma, L. Ren, J. Tong, Z. Liu, L. Xie, Preparation and characterization of surface crosslinked TPS/PVA blend films, Carbohydr. Polym. 76 (2009) 632–638. https://doi.org/10.1016/j.carbpol.2008.11.028.

[78] L. Fu, J. Zhang, G. Yang, Present status and applications of bacterial cellulose-based materials for skin tissue repair, Carbohydr. Polym. 92 (2013) 1432–1442. https://doi.org/10.1016/J.CARBPOL.2012.10.071.

[79] C.I.R. De Oliveira, V.P. De Almeida, M.C.G. Rocha, J.T. De Assis, Evaluation of the effect of compatibilizing agent (PP-g-MA) on PP/Thermoplastic starch blends, Rev. Mater. 24 (2019). https://doi.org/10.1590/s1517-707620190003.0751.

[80] A.M. Senna, J. Braga Do Carmo, J.M. Santana Da Silva, V.R. Botaro, Synthesis, characterization and application of hydrogel derived from cellulose acetate as a substrate for slow-release NPK fertilizer and water retention in soil, J. Environ. Chem. Eng. 3 (2015) 996–1002. https://doi.org/10.1016/j.jece.2015.03.008.

[81] A.A. Sapalidis, Porous Polyvinyl alcohol membranes: Preparation methods and applications, Symmetry (Basel). 12 (2020). https://doi.org/10.3390/SYM12060960.

[82] M.M. Gomaa, C. Hugenschmidt, M. Dickmann, E.E. Abdel-Hady, H.F.M. Mohamed, M.O. Abdel-Hamed, Crosslinked PVA/SSA proton exchange membranes: Correlation between physiochemical properties and free volume determined by positron annihilation spectroscopy, Phys. Chem. Chem. Phys. 20 (2018) 28287–28299. https://doi.org/10.1039/c8cp05301d.

[83] T. Fattahi Meyabadi, F. Dadashian, G. Mir Mohamad Sadeghi, H. Ebrahimi Zanjani Asl, Spherical cellulose nanoparticles preparation from waste cotton using a green method, Powder Technol. 261 (2014) 232–240. https://doi.org/10.1016/j.powtec.2014.04.039.

[84] M. Roman, W.T. Winter, Effect of sulfate groups from sulfuric acid hydrolysis on the thermal degradation behavior of bacterial cellulose, Biomacromolecules. 5 (2004) 1671–1677. https://doi.org/10.1021/bm034519+.

[85] M.N.A.M. Taib, W.A. Yehye, N.M. Julkapli, Influence of Crosslinking Density on Antioxidant Nanocellulose in Bio-degradation and Mechanical Properties of Nitrile Rubber Composites, Fibers Polym. 20 (2019) 165–176. https://doi.org/10.1007/s12221-019-8575-y.

[86] M.B. Gawande, A. Goswami, F.X. Felpin, T. Asefa, X. Huang, R. Silva, X. Zou, R. Zboril, R.S. Varma, Cu and Cu-Based Nanoparticles: Synthesis and Applications in Catalysis, Chem. Rev. 116 (2016) 3722–3811. https://doi.org/10.1021/acs.chemrev.5b00482.

[87] H. Gupta, H. Kumar, M. Kumar, A.K. Gehlaut, A. Gaur, S. Sachan, J.-W. Park, Synthesis of biodegradable films obtained from rice husk and sugarcane bagasse to be used as food packaging material, Environ. Eng. Res. 25 (2019) 506–514. https://doi.org/10.4491/eer.2019.191.

[88] J. Wang, N. Cai, V. Chan, H. Zeng, H. Shi, Y. Xue, F. Yu, Antimicrobial hydroxyapatite reinforced-polyelectrolyte complex nanofibers with long-term controlled release activity for potential wound dressing application, Colloids Surfaces A Physicochem. Eng. Asp. 624 (2021) 126722. https://doi.org/10.1016/j.colsurfa.2021.126722.

[89] A. Deng, Y. Yang, S. Du, X. Yang, S. Pang, X. Wang, S. Yang, Preparation of a recombinant collagen-peptide (RHC)-conjugated chitosan thermosensitive hydrogel for wound healing, Mater. Sci. Eng. C. 119 (2021) 111555. https://doi.org/10.1016/j.msec.2020.111555.

[90] N. Devi, J. Dutta, Development and in vitro characterization of

chitosan/starch/halloysite nanotubes ternary nanocomposite films, Int. J. Biol. Macromol. 127 (2019) 222–231. https://doi.org/10.1016/j.ijbiomac.2019.01.047.

[91] S. Zhang, H. Zhao, Preparation and properties of zein–rutin composite nanoparticle/corn starch films, Carbohydr. Polym. 169 (2017) 385–392. https://doi.org/10.1016/j.carbpol.2017.04.044.

[92] P. Nallasamy, T. Ramalingam, T. Nooruddin, R. Shanmuganathan, P. Arivalagan, S. Natarajan, Polyherbal drug loaded starch nanoparticles as promising drug delivery system: Antimicrobial, antibiofilm and neuroprotective studies, Process Biochem. 92 (2020) 355–364. https://doi.org/10.1016/j.procbio.2020.01.026.

[93] N.K. Rajendran, S.S.D. Kumar, N.N. Houreld, H. Abrahamse, A review on nanoparticle based treatment for wound healing, J. Drug Deliv. Sci. Technol. 44 (2018) 421–430. https://doi.org/10.1016/j.jddst.2018.01.009.

[94] A. Zerboni, R. Bengalli, G. Baeri, L. Fiandra, T. Catelani, Mixture Effects of Diesel Exhaust and Metal Oxide Nanoparticles in Human Lung A549 Cells, (2019) 1–21. https://doi.org/10.3390/nano9091302.

[95] P.E. Antezana, S. Municoy, C.J. Pérez, M.F. Desimone, Collagen Hydrogels Loaded with Silver Nanoparticles and Cannabis Sativa Oil, Antibiotics. 10 (2021). https://doi.org/10.3390/antibiotics10111420.

[96] R. Vazquez-Muñoz, B. Borrego, K. Juárez-Moreno, M. García-García, J.D. Mota Morales, N. Bogdanchikova, A. Huerta-Saquero, Toxicity of silver nanoparticles in biological systems: Does the complexity of biological systems matter?, Toxicol. Lett. 276 (2017) 11–20. https://doi.org/10.1016/j.toxlet.2017.05.007.

[97] M. Palani, S. Kalaiselvan, J. Abel, M. Mark, K. Chandran, V. Ekhambaram, Aspects of Molecular Medicine Green synthesis of CuO nanoparticles : A promising role of antioxidant and antimicrobial activity by using Tribulus terrestris L, Asp. Mol. Med. 4 (2024) 100049. https://doi.org/10.1016/j.amolm.2024.100049.

[98] P. Methylene, B. Dye, A. Yasin, U. Fatima, S. Shahid, S. Mansoor, H. Inam, M. Javed, A. Farouk, Fabrication of Copper Oxide Nanoparticles Using Passiflora edulis Extract for the Estimation of Antioxidant Potential and, (2022) 1–16.

[99] K. Ssekatawa, D.K. Byarugaba, M.K. Angwe, E.M. Wampande, F. Ejobi, E. Nxumalo, M. Maaza, J. Sackey, Phyto-Mediated Copper Oxide Nanoparticles for Antibacterial , Antioxidant and Photocatalytic Performances, 10 (2022) 1–17. https://doi.org/10.3389/fbioe.2022.820218.

São José dos Campos, January 6th, 2025.

Dear Editor,

Attached is our manuscript, entitled "Nanostructured TPS/PVA/CNC Films for Sustained Copper Oxide Nanoparticle Release: Toward Advanced Transdermal Dressing Systems", which we have sent for your consideration for publication in the International Journal of Pharmaceutics.

The present study proposes an innovative approach to the development of transdermal dressing, using starch, from concept to application-focused analysis. The nanocomposite was optimized by selecting biopolymers, adjusting CNC and NPCuO contents, and standardizing the production method to ensure reproducibility. Comprehensive characterization confirmed its swelling, flexibility, permeability, controlled release, and cytocompatibility. The resulting material stands out as a sustainable, low-cost, and biodegradable alternative with strong potential for biomedical applications.

Therefore, we believe that the results and approaches carried out in the manuscript should be communicated to the widest possible audience of materials scientists and other researchers interested in the development of transdermal dressing. There is no better journal than the International Journal of Pharmaceutics for this purpose.

Best regards.

Amanda de Sousa Martinez de Freitas, PhD
amandasmf91@gmail.com

Graphical Abstract (for review)

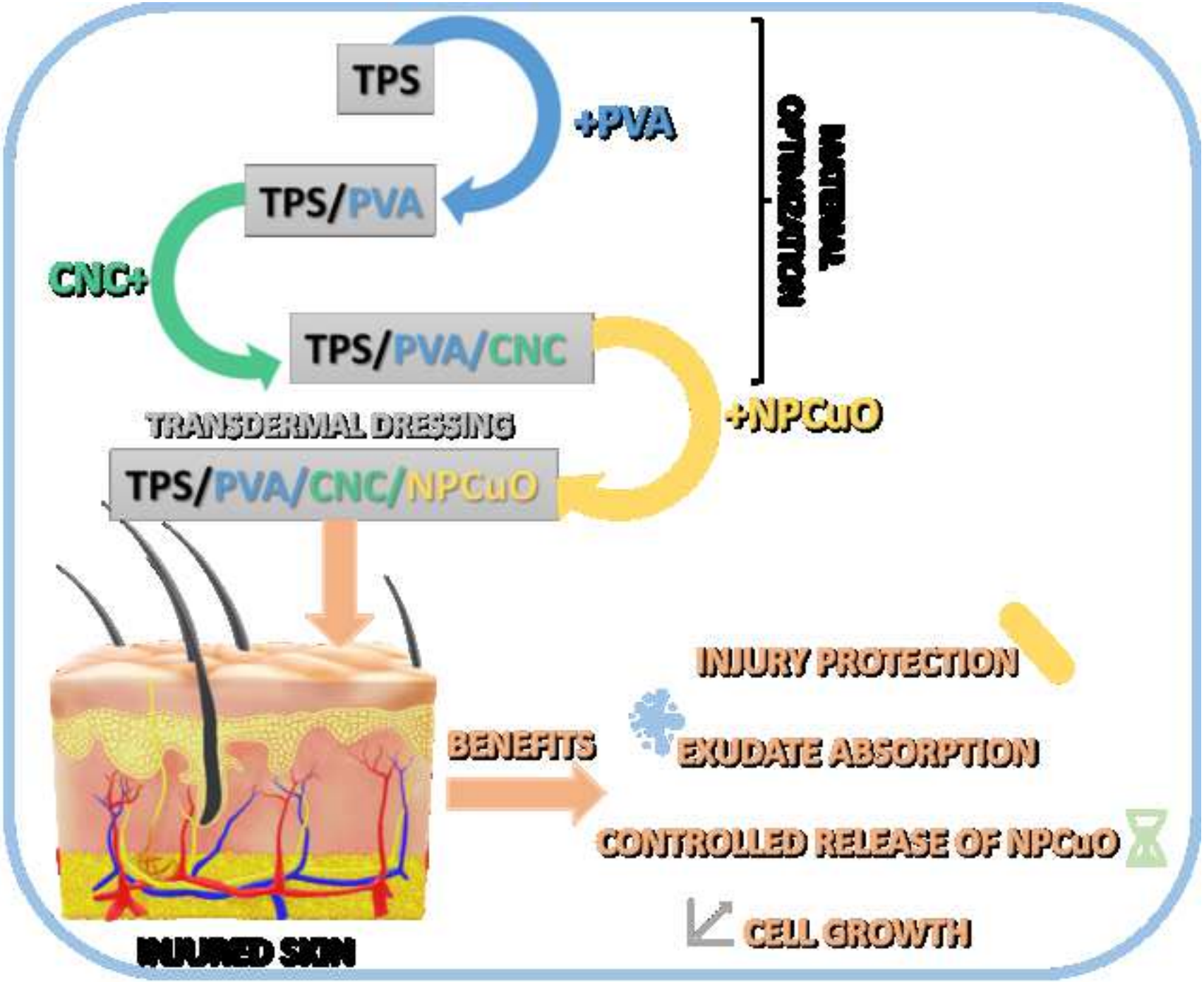

Declaration of interests

☒ The authors declare that they have no known competing financial interests or personal relationships that could have appeared to influence the work reported in this paper.

☐The authors declare the following financial interests/personal relationships which may be considered as potential competing interests:

Nanostructured TPS/PVA/CNC Films for Sustained Copper Oxide Nanoparticle Release: Toward Advanced Transdermal Dressing Systems

Amanda de S. M. de Freitas[a,b*], Jéssica de S. Rodrigues[b], Sofia Municoy[c], Pablo E. Antezana[c], María Laura Foresti[d], Martín F. Desimone[c], Marystela Ferreira[b], Ana Paula Lemes[a]

[a] Polymers and Biopolymers Technology Laboratory (TecPBio), Institute of Science and Technology (ICT), Federal University of São Paulo (UNIFESP), São José do Campos, Brazil

[b] Science and Technology Center for Sustainability (CCTS), Federal University of São Carlos (UFSCar), Sorocaba, Brazil

[c] Institute of Chemistry and Drug Metabolism (IQUIMEFA), University of Buenos Aires (UBA), National Council for Scientific and Technical Research (CONICET), Faculty of Pharmacy and Biochemistry, Buenos Aires, Argentina

[d] Instituto de Tecnología em Polímeros y Nanotecnología, University of Buenos Aires (UBA), National Council for Scientific and Technical Research (CONICET), Laboratorio de Materiales y Estructuras (LAME), Buenos Aires, Argentina

[*]Corresponding author: amandasmf91@gmail.com

Highlights

- Biodegradable nanocomposite films for transdermal dressings with active release.
- Starch-based films with PVA and CNC offer swelling, flexibility, and permeability.
- Copper oxide nanoparticles ensure controlled release in optimized nanocomposites.
- T/P/10CNC/NPCuO films show cytocompatibility, promoting cell proliferation for 48h.
- Innovative dressing material with biodegradability, performance, and low-cost.